ISAS - INTERNATIONAL SCHOOL
FOR ADVANCED STUDIES

A REVIEW ON GRAVITATIONAL LENSING

Thesis submitted for the degree of
Magister Philosophiae

Candidate: V. Faraoni

Supervisor: Prof. G. F. R. Ellis

Academic Year 1988-89

TRIESTE

SISSA - SCUOLA
INTERNAZIONALE
SUPERIORE
STUDI AVANZATI
TRIESTE
Strada Costiera 11

A REVIEW ON GRAVITATIONAL LENSING

Thesis submitted for the degree of
Magister Philosophiae

International School for Advanced Studies

October 1989

CONTENTS

INTRODUCTION

Research in gravitational lensing greatly expanded after the discovery of 0957+561 ten years ago; today many observed objects are explained by gravitational lensing: multiple quasars, blue arcs in rich clusters of galaxies and radio rings; many other of these objects will probably be discovered in the future. Theoreticians produced a physically very reasonable theory of lensing based on the very basic phenomenon of light deflection in weak fields, and applied it to many situations of astrophysical interest. On the other hand, observers found in the sky many objects whose features are described by gravitational lensing, and made great efforts to provide details useful to better understand their structure. Here we will review the present status of theory and observations: chapter 1 examines the standard theory of lenses, points out the commonly used approximations and the three standard formalisms that are used to describe lenses in different contexts: the vector, scalar and propagation formalisms. A topological classification of multiple images and the relation between lens caustics and catastrophe theory are also reported. The known results on multiple imaging are listed, and the possibility of obtaining giant arcs like the observed ones is examined by taking into account both analytical and numerical works. A section is devoted to microlensing, i.e. lensing by small mass objects, that could give high amplification isolated events (and consequently very bright sources), or influence the light curves in a way that has not yet been understood satisfactorily. One can consider events caused by isolated microlenses or by statistical ensembles of microlenses. Finally, the probability of lensing by real objects in a model universe is investigated, and expectation values are predicted for the quantities observable by astronomers. Comparison with the observations must however wait for large enough, statistically useful, samples of gravitational lens systems.

Chapter 2 reviews the observations of gravitational lens candidates: the multiple image systems, the recently discovered giant arcs and radio rings, taking into account the most significative objects. Five multiple systems are to be considered strong candidates, while some others require unreasonable masses or the presence of dark matter; in many cases further observations are needed. A particularly promising class of objects is that of arcs and rings that should permit mapping the mass distribution in the lens with good accuracy; this does not happen for currently known multiple systems, for which one cannot obtain a unique lens model given a image configuration.

Observations of multiple image systems raised a problem of the number of images: this is examinated in chapter 3, together with some possible solutions. Another problem considered in this chapter is the statistical association between galaxies and quasars. Other topics considered in chapter 3 are the evidence for dark matter provided by lensing, the possibility that lensing strongly influences our images of AGNs, and the possible relations between lensing and γ-ray bursts. A section is devoted to the possibility of determining the Hubble parameter H_0 by measuring time delays between different images of multiple systems. Other topics considered are the possibility of detecting cosmic strings through their lensing action on galaxies, the (poorly understood) effect of lenses on the anisotropies of the cosmic microwave background, and a possible explanation of superluminal sources using lenses.

Unless otherwise specified, we will use units in which $G = c = 1$.

Chapter 1

THEORY

1.1 THE CONCEPT OF GRAVITATIONAL LENS

Gravitational deflection of light was predicted by General Relativity before its observation. Its confirmation by Eddington and collaborators in the 1919 eclipse made a great impact.

Let us consider the trajectory of a photon with affine parameter λ in the Schwarzschild's metric:

$$ds^2 = -(1 - \frac{2M}{r})dt^2 + (1 - \frac{2M}{r})^{-1}dr^2 + r^2 d\Omega^2$$

where $d\Omega^2$ is the line element on the unit 2-sphere. With coordinates chosen appropriately, the components of the photon 4-momentum are:

$$p_0 = -E \tag{1.1}$$

$$p_r = (1 - \frac{2M}{r})^{-1}\frac{dr}{d\lambda} \tag{1.2}$$

$$p_\theta = 0 \tag{1.3}$$

$$p_\varphi = L \tag{1.4}$$

$$p^0 = (1 - \frac{2M}{r})^{-1}E \tag{1.5}$$

$$p^r = \frac{dr}{d\lambda} \tag{1.6}$$

$$p^\theta = 0 \tag{1.7}$$

$$p^\varphi = \frac{L}{r^2} = \frac{d\varphi}{d\lambda} \tag{1.8}$$

where E and L are constants along the trajectory (due to the existence of Killing vectors). The equation of the photon trajectory:

$$p_\mu p^\mu = 0$$

becomes:

$$(\frac{dr}{d\lambda})^2 = E^2 - (1 - \frac{2M}{r})\frac{L^2}{r^2} \tag{1.9}$$

By combining eqs.(1.9)and(1.8) we get:

$$\frac{d\varphi}{dr} = \frac{L}{r[E^2 - (1 - \frac{2M}{r})\frac{L^2}{r^2}]^{1/2}} \tag{1.10}$$

We introduce the "impact parameter" $b \equiv L/E$ and the variable $u \equiv r^{-1}$ and get:

$$\frac{d\varphi}{du} = \frac{1}{(1/b^2 - u^2 + 2Mu^3)^{1/2}} \tag{1.11}$$

where the u^3-term describes the relativistic effects. We assume now that M/r is small everywhere along the trajectory and, neglecting terms of order(Mu^2), we find:

$$\frac{d\varphi}{dy} = \frac{1 + 2My}{(1/b^2 - y^2)^{1/2}} + O(M^2u^2) \tag{1.12}$$

where $y \equiv u(1 - Mu)$. The integral of eq.(1.12) is:

$$\varphi = \varphi_0 + \frac{2M}{b} + \arcsin(by) - 2M(\frac{1}{b^2} - \frac{1}{y^2})^{1/2}$$

Here φ_0 determines the incoming direction (since the initial trajectory has $y \to 0$ and $\varphi \to 0$). The photon reaches its smallest radius at

$$y = \frac{1}{b} + O(M^2u^2)$$

(as can be seen by setting $\frac{dr}{d\lambda} = 0$). Since

$$\varphi(b^{-1}) = \varphi_0 + \frac{2M}{b} + \frac{\pi}{2}$$

at its closest approach the photon passed through an angle $\frac{\pi}{2} + \frac{2M}{b}$; by symmetry, going again to infinity the photon path is deflected through twice this angle.

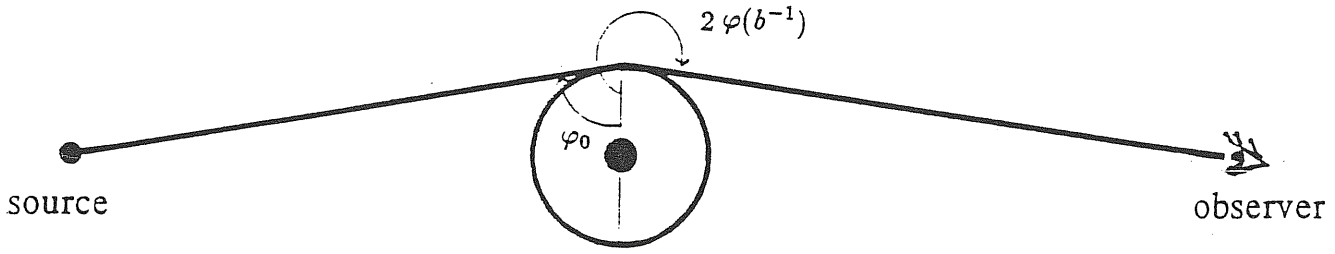

Fig.1

The net deflection is then given by Einstein's formula:

$$\Delta\varphi = \frac{4GM}{c^2 b} \tag{1.13}$$

where we restored G and c. Eq.(1.13) shows some basic properties of gravitational lensing:

- eq.(1.13) has been deduced in an approximation to the full theory and is *linear* ; bending angles due to different masses are additive, so formalisms based on this formula seem to be set in the framework of linearized General Relativity, at least as concerns the effects of clumpiness of matter in the universe;
- the deflection angle does not depend on the photon's frequency, so

  gravitational lenses are achromatic

- different null geodesics from a light source can pass on opposite sides of the deflecting object and intersect each other after deflection, so an observer collecting these light rays will see several images coming from apparently different directions.

Bending of light rays is a general concept in General Relativity: photons' trajectories depart from straight lines (in space) according to the matter distribution and the topology of the universe. In this broad sense any local departure from a smooth model universe can be called "gravitational lens"; however astronomers use this term to denote more specific situations in which an object located at a well defined position in the sky focuses light rays from a source at cosmological distance, with multiple imaging or significant amplification. Possible sources of astrophysical interest are quasars (QSOs), active galactic nuclei (AGNs), galaxies, γ-ray bursts (GRBs), cosmic microwave background (CMB) anisotropies, supernovae in galaxies, etc. Different objects can act as lenses in real life, on different angular scales that can be estimated using eq.(1.13) and assuming the lens size as impact parameter. Lensing by an object with mass $M \sim M_\odot$ (a normal or collapsed star, or a non-massive black hole) is called *microlensing*, and the angular deflection scale is:

$$\alpha \sim 1.75(\frac{M}{M_\odot})(\frac{b}{R_\odot})\ arcseconds$$

Microlensing is actively studied because of its very peculiar features. We may call *millilensing* the gravitational lensing by objects with mass between stellar and galactic ones, such as globular clusters, giant molecular clouds, or $\sim 10^6 M_\odot$ halo black holes. The angular scale for such objects is $\alpha \sim 10^{-3}$ arcseconds. The term *macrolensing* (or simply lensing) is used when the deflector is a galaxy, a galaxy cluster or a more massive object (supercluster or cosmic string). The angular scale is $\alpha \sim 1'' - 10''$ (and up to $100''$ for cosmic strings). Observations of gravitational lensing concern multiply imaged systems, giant luminous arcs in rich clusters of galaxies, radio rings and statistical galaxy-QSO association. The important effects of a gravitational lens are not only splitting of images and deflection of light rays, but also amplification, distortion and rotation of images, and time delay between different images.

1.2 HISTORICAL NOTES

The concept of gravitational lens was at first a purely theoretical one; only a long time after its introduction it became an observed reality. A brief history of gravitational lenses:

- 1916: the light deflection of 1.75″ at the solar limb is predicted by General Relativity;
- 1919: Eddington observes the predicted deflection;
- Einstein considers lensing of a star by another star and discovers the Einstein ring and the amplification effect; he concludes that the probability of observing such a phenomenon is very low;
- Zwicky realizes that gravitational lensing by a *galaxy* is much more efficient, and considers galaxies as sources;
- early 1960's: many theoretical studies;
- 1963: discovery of the first QSO. People realize that QSOs can be ideal sources for gravitational lensing due to their distance and brightness;
- 1965: Barnothy tries to interprete *all* QSOs as gravitationally lensed Seyfert I nuclei;
- 1975: Bourassa-Kantowski formalism for mass density distributions;
- 1979: discovery of the first multiply imaged system 0957+561;
- An impressive amount of theoretical and observational papers appear. Today we have about twenty candidates for multiply imaged systems.
- 1987: discovery of the giant luminous arcs A370 and Cl2244-02;
- 1988: discovery of the radio ring MG1131+0456

1.3 ORDER OF MAGNITUDE ESTIMATES

Rough estimates can be obtained considering an extremely simplified situation in euclidean space as follows:

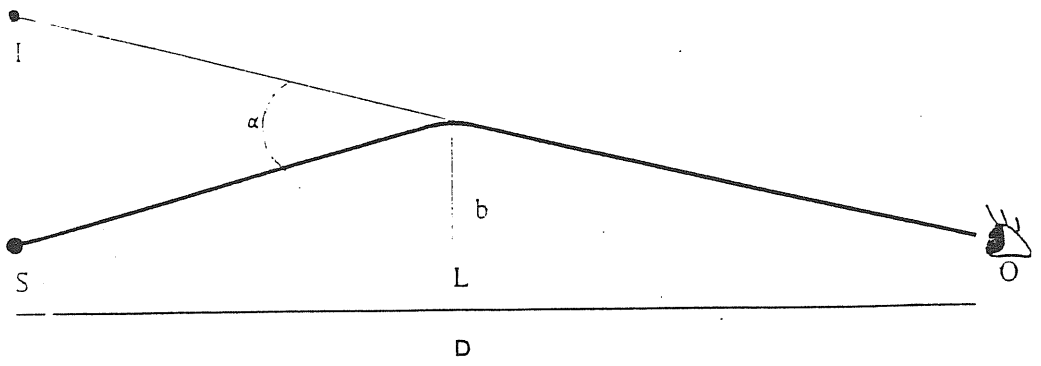

Fig. 1

S source

L lens

O observer

I image

D source distance

R lens size

b impact parameter

α deflection angle

1.3.1 Bending angle

Einstein's formula permits one to estimate the angular deflection scale of a light ray with impact parameter b by a lens of mass M. This is also the scale of separation in multiply imaged systems. If we model the lens galaxy with an isothermal sphere, we get [Gott, 1987] :

$$\alpha = 2.6(\frac{\sigma}{300kms^{-1}})^2 \ \ arcseconds$$

(where σ is the one-dimensional velocity dispersion) so we can write:

$$\alpha \sim \frac{M}{b} \sim \sigma^2 \tag{1.14}$$

1.3.2 Condition for multiple imaging

The rough condition to have multiple imaging is:

$$image - source \ \ separation \geq lens \ \ size$$

$$\alpha D \geq R$$

This condition can be set as a condition on the matter surface density Σ in the lens:

$$\Sigma \sim \frac{M}{R^2} \sim \frac{\alpha}{R} \geq \frac{1}{D}$$

There is a critical density $\Sigma_c \sim \frac{c^2}{4\pi GD}$ for multiple imaging; galaxies can have supercritical densities, while clusters usually cannot.

1.3.3 Time delays

Different light rays deflected by the same lens travel along different paths and reach an observer with a time delay that is roughly given by the Schwarzschild radius of the lens [Blandford and Kochanek, 1988] :

$$\Delta t \sim M \sim \alpha R \sim \alpha(\alpha D) = \alpha^2 D \sim \frac{\theta^2 D}{4} \tag{1.15}$$

where $\theta \sim 2\alpha$ is the image separation.

1.3.4 Probability of lensing

According to Press and Gunn [1973], let n be the lens number density ; then the optical depth of the universe to lensing is roughly:

$$\tau \sim nR^2 D$$

Since

$$\alpha D \sim R$$

$$\frac{MD}{R} \sim \alpha D \sim R$$

$$R^2 \sim MD$$

and

$$\rho_c = \frac{3H^2}{8\pi} \sim \frac{1}{D^2}$$

we get:

$$nR^2 D \sim nMD^2 \sim \frac{\rho_{lens}}{1/D^2} \sim \frac{\rho_{lens}}{\rho_c}$$

or

$$\tau \sim \Omega_{lens} \tag{1.16}$$

Thus, for galaxies, $\tau_{gal} \sim 0.01$.

1.4 APPROXIMATIONS AND DIFFERENT APPROACHES

1.4.1 APPROXIMATIONS

Many approximations are currently used in gravitational lens theory and it is important to check if the assumptions hold in realistic cases (for example this could be the case for the odd image theorem and the "missing image problem" - see later). The most common assumptions in the literature are the following:

Geometric optics approximation

Roughly speaking, diffraction effects are important only if the radiation wavelength is of the order, or greater than the Schwarzschild radius of the lens:

$$\lambda \geq R_s$$

For lensing galaxies or galaxy clusters and radio (or greater wavelength) waves we have: $\lambda << R_s$ <length scale of variation of the lensing potential. Even for the Sun ($R_s \sim 3Km$) diffraction is important only for waves with frequencies $\nu \leq 100KHz$; so diffraction usually is not important for conventional waves. This could not be the case if we consider lensing *of gravitational waves* by ordinary lenses: very long gravitational waves (present period $P_o < 10^{-3}s$) of primordial origin are often considered in studies on the gravitational wave background [Carr, 1980; Rosi and Zimmerman, 1976] ; diffraction would be important for such waves. One could also consider lensing *by gravitational waves* instead of ordinary lenses; in this case diffraction becomes important when the space and time scales of variation of the lensing (gravitational) wave are of the order of the wavelength (or period) of the lensed (electromagnetic) wave.

Thin screen approximation

When single lenses are considered, it is commonly assumed that the transverse distance between the deflected and the undeflected ray is much smaller than the length scale of variation of the lensing potential, i.e. one assumes the lens lies at a single, definite redshift. However double or multiple lenses can be considered in not-unrealistic cases [Crawford *et al.*,1986; Nemiroff, 1988; Kovner, 1987*c*].

Transparency of the lens

It is usually assumed that the gravitational lens is transparent[1], i.e. every photon path traverses the lens. However, in multiple imaging situations, one can dim one image as one wants by increasing the compactness of the lens nucleus and, in the limit, turn the image off by making the lens singular. Actual galaxies, halos or clusters can contain gas that absorbs or scatters photons from a light beam, so the transparency assumption can be unrealistic in some cases.

[1] except for singular lenses

Paraxial approximation

It is customary to consider small deflection angles. Observed separations in multiple images of almost all systems (of the order of the deflection angles) are of some arcseconds. Much wider deflections (or splittings) would require unreasonable lens masses.

Lens stationarity

Almost all works on gravitational lensing assume that the deflector is static. This is certainly adequated for ordinary lenses such as galaxies, clusters, or stars, but could not be valid for lensing by rapidly vibrating black holes, or by gravitational waves.

The lens is bounded

It is assumed that, if Φ is the newtonian potential of the lens, Φ and $\underline{\nabla}\Phi$ become zero at infinity. This is reasonable for all conventional lenses.

1.4.2 DIFFERENT APPROACHES

Three main approaches to gravitational lens theory can be found in the literature: the **vector formalism** is the most common and seems the most well-suited to treat point-like lenses (e.g. in microlensing). It is sometimes called "newtonian approach", because it describes deflection of rays with linearized General Relativity and the lens by newtonian theory. Cosmology must be included in the model, since realistic sources and lenses are at cosmological distances: this is done by using the relativistic angular diameter distances as distance measures. This is probably correct since angular quantities are measured in observations; however mixing exact relativistic cosmology and linearized theory is not satisfactory in principle.

The **scalar formalism** is based on Fermat's principle, which is valid in linearized General Relativity (and, in a suitable form, in arbitrary gravitational fields [Kovner, 1988]). This formalism allows a topological classification of multiple images using catastrophe optics. It also uses angular diameter distances to describe cosmology.

The **propagation formalism** is based on the relativistic optical scalar equations (OSE) ; they are useful in considering inhomogeneous universes with no well-defined lens planes at which light rays are bent. Actually the term "propagation formalism" includes more than one approach based on relativistic OSE.

THE VECTOR FORMALISM

The vector formalism [Bourassa *et al.*, 1973; Bourassa and Kantowski, 1975] assumes the following:

- linearized General Relativity
- geometric optics
- small-angle scattering

- transparent, bounded, and stationary lenses
- thin screen approximation

The propagation of a photon through the universe and the lens field is described by a mapping from the *image plane* (the sky as we see) to the *source plane* (the sky as it would look were the lens absent). The image plane is taken orthogonal to the source-observer line of sight, and passing through the lens; the source plane is analogously defined, passing through the source. Cartesian coordinates $\underline{r} = (x, y)$ and $\underline{s} = (s_x, s_y)$ are used for the image and source positions respectively. The mapping is defined *from the observer* to the source because one wants to have a single-valued function even in case of multiple imaging. The origin of coordinates in the sky is determined by a conveniently chosen optic axis. $\underline{s}$ can be defined as the image coordinate in the image plane, were the lens absent.

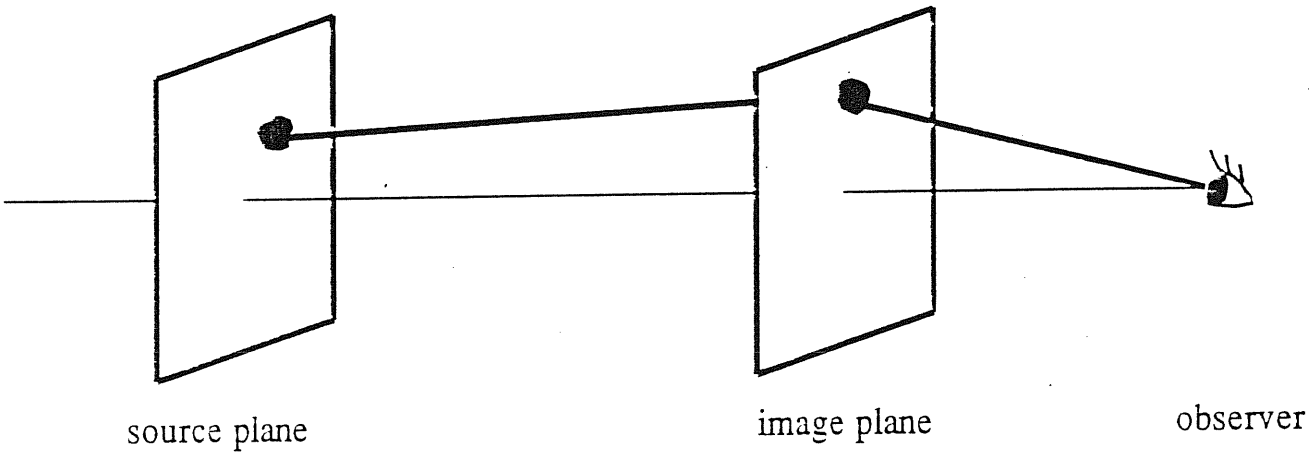

Fig. 3.

Let us consider the linear positions of the source and the image *in the source plane*; they are obtained from the linear positions in the image plane and the angles they subtend, as seen by the observer:

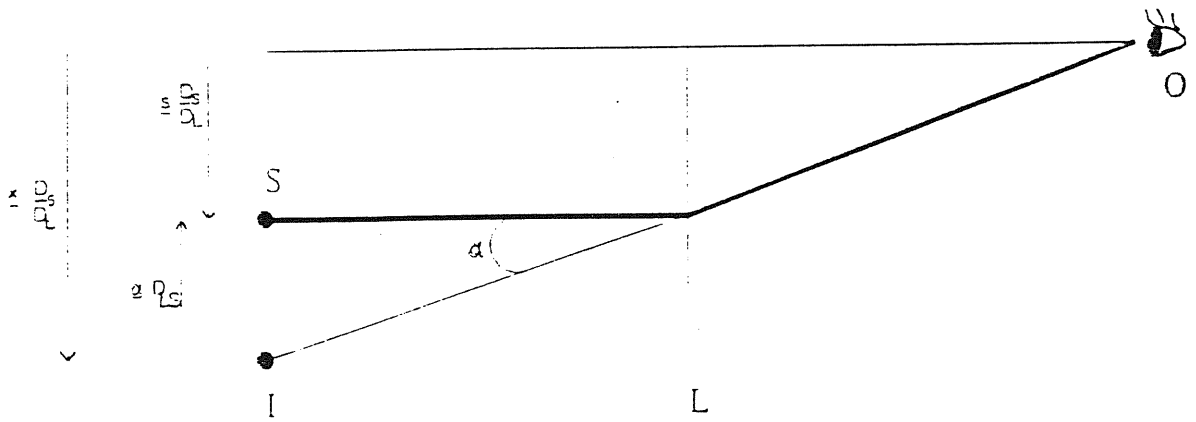

Fig.4

$\underline{x}\frac{D_S}{D_L}$ image linear position in the source plane

$\underline{s}\frac{D_S}{D_L}$ source linear position in the source plane

$\underline{\alpha}D_{LS}$ linear deflection in the source plane

D_L observer-lens distance

D_S observer-source distance

D_{LS} lens-source distance

we get:

$$\underline{x}\,\frac{D_S}{D_L} = \underline{s}\,\frac{D_S}{D_L} + (-\underline{\alpha})D_{LS}$$

Introducing

$$D \equiv \frac{D_L D_{LS}}{D_S} \tag{1.17}$$

we get the **lens equation**:

$$\underline{s} = \underline{x} + D\underline{\alpha} \tag{1.18}$$

where the deflection angle $\underline{\alpha}$ can be obtained from linearized General Relativity considering the path of a photon with 4-momentum:

$$p^\mu = (1, \delta p^1, \delta p^2, 1) = \frac{dx^\mu}{d\lambda}$$

suffering a net deflection:

$$\Delta p^\mu = -\int d\lambda (h^\mu_{\lambda,\lambda} - \frac{1}{2} h_{\lambda\lambda}{}^{,\mu}) = -\frac{2}{c^2}\int d\lambda \Phi^{,\mu} + O[(\delta p)^2]$$

that gives for the bending angle:

$$\underline{\alpha} = -\frac{2}{c^2}\int d\underline{l} \nabla \Phi \tag{1.19}$$

where the integral is taken along the unperturbed photon's path between the source and the observer. In the approximation employed, $\underline{\alpha}$ is a 2-dimensional vector with no component parallel to the photon's path, and depending on the projected, 2-dimensional, structure of the lens. The angular diameter distances in the Friedmann-Robertson-Walker universe are used for the Ds to describe cosmology. The angular diameter distance between two objects at redshifts z_A and z_B (with $z_A < z_B$) is given by Weinberg [1972] :

$$D_{AB} = \frac{2}{H_0}\frac{(1-\Omega_0)(G_A - G_B) + (G_A G_B^2 - G_A^2 G_B)}{\Omega_0^2 (1+z_A)(1+z_B)^2} \tag{1.20}$$

where

$$G_i = (1 + \Omega_0 z_i)^{1/2} \quad i = A, B$$

and H_0, Ω_0,and q_0 are the present Hubble parameter, density parameter, and deceleration parameter respectively. Results in gravitational lensing are more sensitive to the choice of the lens model than to the choice of Ω_0. A $\Omega_0 = 1$ ($k = 0$) Einstein-De Sitter model is most commonly used in literature. The transformation described by the lens equation has the jacobian matrix:

$$J(\underline{x}) = \frac{\partial \underline{s}}{\partial \underline{x}}$$

Its inverse represents the *amplification tensor*:

$$A(\underline{x}) \equiv \frac{\partial \underline{x}}{\partial \underline{s}}$$

whose determinant is the scalar amplification:

$$\mathcal{A} \equiv Det(\frac{\partial \underline{x}}{\partial \underline{s}})$$

The loci of points in the image plane in which $Det(J) = 0$ are *critical lines* and the corresponding lines in the source plane are called *caustics*. They separate regions in the source plane corresponding to different numbers of images; as a point source is moved in the source plane, images appear or disappear in pairs when the source crosses a caustic. Amplification is virtually infinite on critical lines; in practice it is limited by wave optics to the values:

$$\mathcal{A} \sim (\frac{GM}{\lambda c^2})^{1/3} \tag{1.21}$$

on a fold caustic, and

$$\mathcal{A} \sim (\frac{GM}{\lambda c^2})^{1/2} \tag{1.22}$$

on a cusp caustic, where M is the lens mass, and the intensification is chromatic [Mc Breen and Metcalfe, 1987] ; A can however be very large. In case of multiple imaging, different images will generally have different amplifications.

Complex notation

The 2-dimensional nature of the bending angle $\underline{\alpha}$ allows the use of complex notation; $\underline{\alpha}$ is replaced by the complex number $\alpha = \alpha_x + i\alpha_y$ and is completely represented by the *scattering function*:

$$I(\underline{x}) = \frac{1}{2G}[\int_{-\infty}^{+\infty} \frac{\partial \Phi(\underline{x}, l)}{\partial x} dl - i \int_{-\infty}^{+\infty} \frac{\partial \Phi(\underline{x}, l)}{\partial y} dl] \tag{1.23}$$

via the expression:

$$\alpha = -\frac{4G}{c^2} I^* \tag{1.24}$$

Eqs. (1.24) and (1.19) are equivalent. One makes also the substitutions:

$$\underline{x} \equiv (x, y) \mapsto z = x + iy$$
$$\underline{s} \equiv (s_x, s_y) \mapsto z_s = s_x + is_y$$

The scattering function $I(z)$ is analytic outside the matter distribution (as can be proved using the Cauchy-Riemann conditions) and its knowledge is equivalent to that of the projected lensing potential. The lens equation is:

$$z_s = z - \frac{4GD}{c^2} I^* \tag{1.25}$$

and can have more than one solution z for a given source position z_s (multiple imaging). The amplification tensor is:

$$A = \frac{\partial z}{\partial z_s} = \frac{1}{\mathcal{G}^2 - |\mathcal{F}|^2} \begin{pmatrix} \mathcal{G} + \mathcal{R}e(\mathcal{F}) & -\mathcal{I}m(\mathcal{F}) \\ -\mathcal{I}m(\mathcal{F}) & \mathcal{G} - \mathcal{R}e(\mathcal{F}) \end{pmatrix} \tag{1.26}$$

where:

$$\mathcal{G} \equiv 1 - \frac{2GD}{c^2}(\partial_x I + i\partial_y I) \tag{1.27}$$

$$\mathcal{F} \equiv \frac{2GD}{c^2}(\partial_x I - i\partial_y I) \tag{1.28}$$

The function $\mathcal{G}$ is real and can be written:

$$\mathcal{G} = 1 - \frac{4\pi GD}{c^2}\Sigma(x,y) \equiv 1 - \chi \tag{1.29}$$

where

$$\Sigma(x,y) \equiv \int_{-\infty}^{+\infty} dl \rho(x,y,l) \tag{1.30}$$

is the projected surface density of the lens and χ (called *convergence*) is the same quantity measured in units of

$$\Sigma_c \equiv \frac{c^2}{4\pi GD} \tag{1.31}$$

We have $\chi \geq 0$ and $\mathcal{G} \leq 1$. $\mathcal{F}$ is a complex function. Clearly, $\mathcal{G} \to 0$ and $|\mathcal{F}| \to 0$ as $r \to \infty$. The eigenvalues of the amplification tensor A are:

$$\lambda_\pm = \frac{\mathcal{G} \pm |\mathcal{F}|}{\mathcal{G}^2 - |\mathcal{F}|^2} \tag{1.32}$$

and are real. Their product is the amplification of the image located at z resulting from a small source located at z_s:

$$\mathcal{A} = \frac{1}{\mathcal{G}^2 - |\mathcal{F}|^2} \tag{1.33}$$

In fact, since surface brightness is conserved by lensing [Etherington, 1933] , the amplification (ratio of intensities with and without the lens) is simply the ratio:

$$\frac{\textit{area of an infinitesimal region in the image plane}}{\textit{area of the corresponding region in the source plane}}$$

A small disk source will be imaged into an ellipse whose eccentricity ϵ is given by the ratio of the eigenvalues of A :

$$(1-\epsilon^2)^{1/2} = |\frac{\lambda_+}{\lambda_-}| = |\frac{\mathcal{G} - |\mathcal{F}|}{\mathcal{G} + |\mathcal{F}|}| \tag{1.34}$$

while the eigenvectors of A give the orientation of the ellipse.

Transverse motions of the source or lens

Relative motion of the source and the lens will cause displacements $\delta\underline{x}$ of the image that can be computed using the lens equation, giving:

$$\delta\underline{x} = A\,\delta\underline{s} \tag{1.35}$$

where $\delta\underline{s}$ is the displacement of the source in the image plane. For source motions it is given by:

$$\delta\underline{s} = \frac{D_L}{D_S}\,\underline{v}_S \delta t_S$$

and for lens motions it is given by:

$$\delta\underline{s} = \underline{v}_L \delta t_L$$

where

$\underline{v}_S$ is the transverse velocity of the source (measured at the emission time t_S)

$\underline{v}_L$ is the transverse velocity of the lens measured at the time t_L the light passes the lens

δt_S is the time interval during which the source moves (measured at emission times t_S)

δt_L is the time interval during which the lens moves (measured at times t_L)

An observer measures a time interval δt_O during which the image moves. We have:

$$\delta t_S = \delta t_O (1 + z_S)^{-1}$$

for source motions and

$$\delta t_L = \delta t_O (1 + z_L)^{-1}$$

for lens motions, where z_S and z_L are the source and lens redshifts respectively. For source motions we get:

$$\delta\underline{x} = A\,\frac{D_L}{D_S}\,\underline{v}_S\,\delta t_O (1 + z_S)^{-1} \tag{1.36}$$

and for lens motions:

$$\delta\underline{x} = A\,\underline{v}_L\,\delta t_O (1 + z_L)^{-1} \tag{1.37}$$

THE SCALAR FORMALISM

This approach [Schneider, 1985; Blandford and Narayan, 1986; Narayan, 1986] assumes the following:

- post-newtonian metric
- geometric optics
- small angle scattering
- thin screen approximation

- bounded and stationary lens

Consider a source at redshift z_S, a lens at redshift z_L and an observer. We use *angular* coordinates $\underline{\theta}_S$ and $\underline{\theta}_I$ for the source and image positions respectively. The path of a light ray in the post-newtonian metric obeys:

$$ds^2 = -(1+2\Phi)dt^2 + (1-2\Phi)dl^2 = 0$$

which gives:

$$dt = (1-2\Phi)dl + O(\Phi^2)$$

The travel time of the photon is obtained by integrating along the (perturbed) photon path from the source to the lens plane (since we use quantities measured in the lens plane):

$$t_L = \int_S^L dl - 2\int_S^L \Phi dl$$

(t_L is the time at which light crosses the lens plane). Using the following geometry

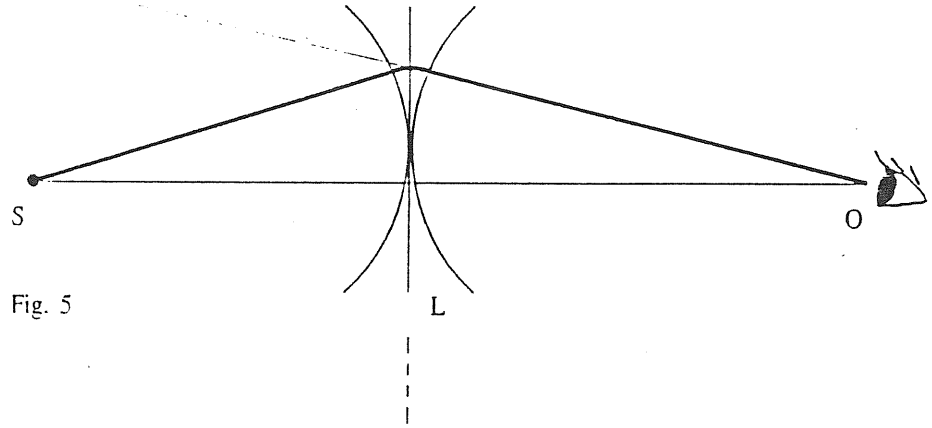

Fig. 5

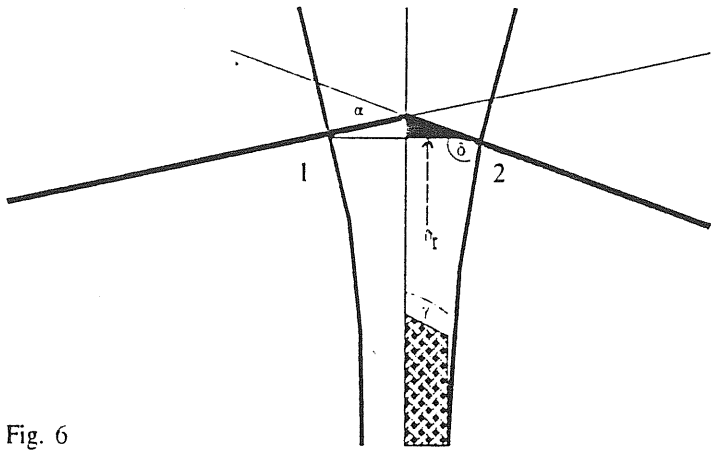

Fig. 6

(where the arcs are contours of constant propagation time) we get the geometrical time delay; the total time delay t_L (measured in the lens plane) is the sum of a geometrical term and a gravitational term (familiar from studies of radar signal propagation in the Solar System [e.g. Will, 1981]) The geometrical time delay is roughly:

$$\Delta l_{1L} = D_L(\theta_I - \theta_S)\sin(\frac{\alpha}{2}) \sim D_L(\theta_I - \theta_S)\frac{\alpha}{2}$$

and, more precisely:

$$\Delta l_{1L} = \frac{1}{2}\underline{\alpha}\cdot D_L(\underline{\theta}_I - \underline{\theta}_S) = \frac{1}{2}\frac{D_L D_S}{D_{LS}}(\underline{\theta}_I - \underline{\theta}_S)^2$$

where the lens equation has been used.Now:

$$\Delta t_L = \Delta t_{Lgeom.} + \Delta t_{Lgrav.} = \frac{D_L D_S}{2D_{LS}}(\underline{\theta}_I - \underline{\theta}_S)^2 - 2\int_S^L \Phi dl$$

Converting to the observer's time:

$$\Delta t(\underline{\theta}_I) = (1+z_L)\,[\frac{D_L D_S}{2D_{LS}}(\underline{\theta}_I - \underline{\theta}_S)^2 - 2\int_S^L \Phi(\underline{\theta}_I)dl] \tag{1.38}$$

We introduce the quantities:

$$\tau \equiv \frac{D_{LS}}{D_L D_S}(1+z_L)^{-1}\Delta t \tag{1.39}$$

$$\Psi(\underline{\theta}_I) \equiv \frac{2D_{LS}}{D_L D_S}\int_S^L dl\Phi(\underline{\theta}_I) \tag{1.40}$$

The potential Ψ satisfies the 2-dimensional Poisson equation:

$$\frac{\partial^2\Psi}{\partial\theta_{I_1}^2} + \frac{\partial^2\Psi}{\partial\theta_{I_2}^2} = 8\pi\frac{D_L D_{LS}}{D_S}\Sigma \equiv 2\frac{\Sigma}{\Sigma_c} \tag{1.41}$$

Eq. (1.38) can be written:

$$\tau(\underline{\theta}_I, \underline{\theta}_S) = \frac{1}{2}(\underline{\theta}_I - \underline{\theta}_S)^2 - \Psi(\underline{\theta}_I) = \tau_{geom.} + \tau_{grav.} \tag{1.42}$$

Fermat's principle states that *for a given source position θ_S, the images are located at the stationary points of τ with respect to variations of $\underline{\theta}_I$*:

$$\frac{d\tau}{d\underline{\theta}_I} = 0 \quad for\ actual\ rays \tag{1.43}$$

Eq. (1.43) gives the lens equation:

$$\underline{\theta}_S = \underline{\theta}_I - \underline{\nabla}\Psi(\underline{\theta}_I) \tag{1.44}$$

or

$$\underline{\theta}_S = \underline{\nabla}\tau(\underline{\theta}_I, 0) \tag{1.45}$$

In a τ-$\underline{\theta}_I$ diagram the geometrical time delay $\tau_{geom.} = \frac{1}{2}(\underline{\theta}_I - \underline{\theta}_S)^2$ is represented by a paraboloid whose minimum at $\underline{\theta}_I = \underline{\theta}_S$ gives the unperturbed single image. Gradually introducing mass, the arrival time surface $\tau(\underline{\theta}_I)$ is raised (since $-\Psi > 0$) and new stationary points are created: they can be minima, maxima, and saddle points and correspond to additional images. The extrinsic curvature of the time delay surface $\tau(\underline{\theta}_I)$:

$$K_{ij} = \delta_{ij} - \frac{\partial^2 \Psi}{\partial \theta_{I_i} \theta_{I_j}} = \frac{\partial \theta_{S_i}}{\partial \theta_{I_j}}$$

is the jacobian of the plane-to-plane transformation given by the lens equation, while its inverse K^{-1} is the amplification tensor. In a coordinate system that diagonalizes the tensor K we have:

$$K = \begin{pmatrix} \frac{1}{\rho_1} & 0 \\ 0 & \frac{1}{\rho_2} \end{pmatrix}$$

where ρ_1 and ρ_2 are the principal radii of curvature of the time delay surface and the eigenvalues of the amplification tensor. Their signs are the *partial parities* of an image; their product is the *amplification*, whose sign is the *total parity* of the image. Three cases are possible:

- at a *minimum* of the time surface the partial parities are $++$ (total parity $+$);
- at a *maximum* the partial parities are $--$ (total parity $+$);
- at a *saddle point* the partial parities are $+-$ (total parity $-$).

In our approximations, the tensor K (and K^{-1}) is symmetric, so images are expanded, sheared, mirror-inverted, but not rotated with respect to the source. One can write:

$$K = \begin{pmatrix} k + \mu & 0 \\ 0 & k - \mu \end{pmatrix}$$

where

$$k \equiv \frac{\rho_1^{-1} + \rho_2^{-1}}{2} = 1 - \frac{\Sigma}{\Sigma_c}$$

and

$$\mu \equiv \frac{\rho_1^{-1} - \rho_2^{-1}}{2}$$

are the *expansion* and the *shear* respectively. k depends only on matter along the line of sight, while μ arises from matter outside the beam. The total amplification is

$$\rho_1 \rho_2 = \frac{1}{k^2 - \mu^2}$$

The point of view of the scalar formalism permits one to immediately arrive at some conclusions:

1. if the lens is absent the time delay surface has only a minimum, then there is only one (positive parity) image. Adding a lens produces new images in pairs of opposite (total) parities, since we can only add a local maximum together with a saddle point at one time. Moreover, if we have $2n+1$ images, $n+1$ have positive total parity and n have negative total parity;

2. the earliest image to arrive corresponds to a global minimum in the time delay surface (since $\tau \in C^0$ and $\tau \to \infty$ as $|\underline{\theta}_I| \to \infty$) and has positive parity;

3. images with positive partial parities ($k+\mu > 0$, $k-\mu > 0$) are amplified. In fact their amplification is
$$\mathcal{A} = \frac{1}{k^2-\mu^2} = \frac{1}{k^2}\,\frac{1}{1-\mu^2/k^2} > \frac{1}{k^2} > 1$$
where we used:
$$k+\mu > 0 \quad and \quad k-\mu > 0$$
from which:
$$|\mu| < k = 1 - \frac{\Sigma}{\Sigma_c} < 1$$

4. the cross section for lensing for a point source in the source plane is:
$$\sigma = \int d^2\theta_S$$
since the amplification tensor A is the jacobian of the plane-to-plane transformation $\underline{\theta}_S \mapsto \underline{\theta}_I$ we get:
$$\sigma = \int \mathcal{A}^{-1} d^2\theta_I$$
(where only one image per source position is included in computing the integral). Roughly we have:
$$\sigma(\mathcal{A}) \propto \mathcal{A}^{-2}$$
(this holds when caustics are dominated by folds).

Topological classification of the images

By considering the level curves of the time delay surface (isochronals) one can give a topological classification of the images according to the number and types of possible extremal points.

3-image topology:

denoting maxima, minima and saddle points of the time surface $\tau(\underline{\theta}_I)$ by H, L and S respectively, one of the three images has to be L and one S. Then we have *only two possible topologies*: LLS and LHS. The shapes of the critical contours are the *lemniscate* and *limacon* curves [Blandford and Narayan, 1986; Blandford and Kochanek, 1988] .

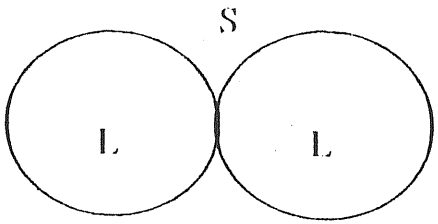

lemniscate

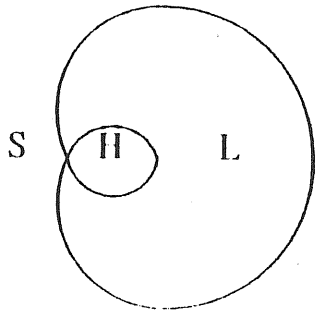

limacon

Fig. 7

The lemniscate occurs with elongated lenses and the limacon when the lens is like a spherical, non-singular galaxy. The limiting cases are when the lens is a string, or a black hole respectively (in the former case the S image is on the string and disappears; in the latter case the H image is on the black hole, and disappears). Consider the lens fixed and move the source around; the images and the critical contour will also move. For the lemniscate case, the caustic curve in the source plane consists of two cusps joined by two smooth curves (fold catastrophes):

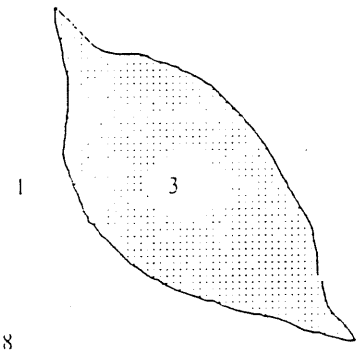

Fig. 8

There are three images when the source is inside the caustic and a single image when the source is outside it. When the source crosses the caustic from inside to outside, two images merge and disappear.

For the limacon case, there are a inner and a outer caustic in the source plane. There are five images when the source is inside the inner caustic, three images when it is between the inner and the outer caustic, and one image when it is outside the outer caustic. The inner caustic consists of four cusps joined by folds. The outer caustic is a pure fold catastrophe.

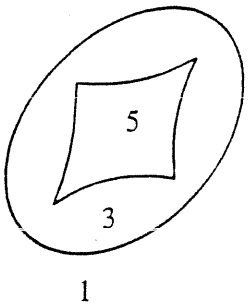

Fig. 9

5-image topology:

there are six possible non-degenerate 5-image topologies, where "degenerate" means that two (or more) saddle points have a common isochronal contour, or that two images merge. The critical contours have the shapes showed in fig.10.

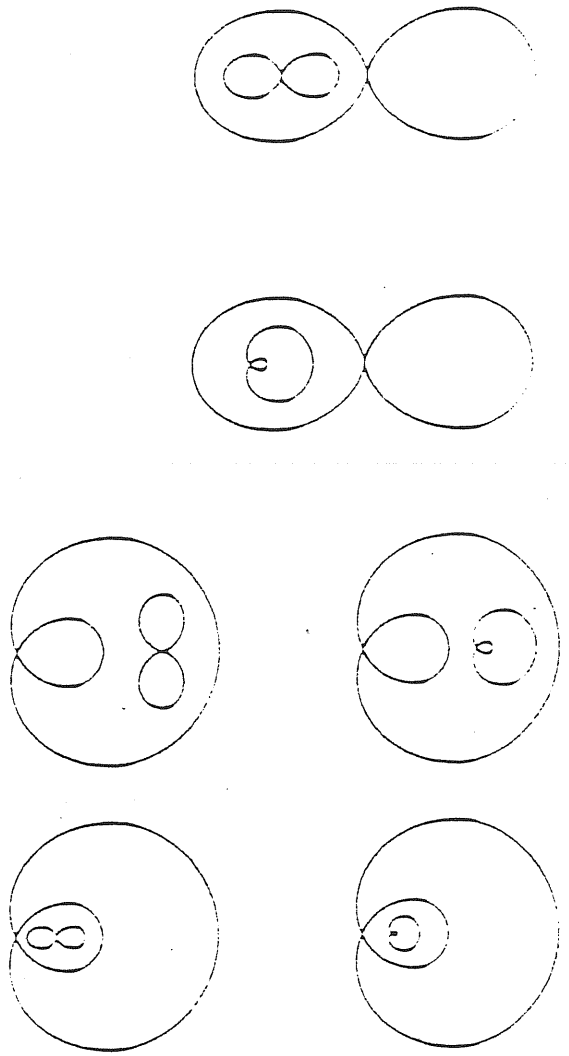

Fig. 10 Crossing contours for 5-image topologies
(from Blandford and Kochanek, 1988)

7 image topology:

in this case there are twenty-five topologically distinct, non-degenerate arrival time surfaces.

Catastrophe theory and caustics

Caustics in the source plane can be described by catastrophe theory [Arnold, 1984; Poston and Stewart, 1978], in a way similar to the optics of glass lenses [Berry and Upstill, 1976]. Transitions are possible from one of the described topologies to another through merger or creation of pairs of images at a caustic. Consider first an isolated image; by choosing suitably the origin of coordinates so that a source at $\underline{\theta}_S = \underline{0}$ gives an image at $\underline{\theta}_I = \underline{0}$, and Taylor-expanding, the time surface $\tau(\underline{\theta}_I)$ locally takes the form:

$$\tau(\underline{\theta}_I) = \frac{a}{2}x_I^2 + \frac{b}{2}y_I^2 + \dots \tag{1.46}$$

where $\underline{\theta}_I = (x_I, y_I)$ and eq.(1.42) implies $a + b \leq 2$. Eqs. (1.45) and (1.46) give the image position for a generic source position $\underline{\theta}_S = (x_S, y_S)$:

$$x_I = \frac{x_S}{a}$$

$$y_I = \frac{y_S}{b}$$

and the mapping is simply a change of scale with different factors a^{-1} and b^{-1} along the two axes. A *fold catastrophe* correspond to a smooth caustic curve. A source on one side of a fold generates two images (on opposite sides of the corresponding critical line in the image plane), while on the other side it generates no images. As the source crosses the fold from the two-image region, two images merge into a very bright one and disappear. In the case of a fold catastrophe the time surface is locally of the form:

$$\tau(\underline{\theta}_I) = \frac{a}{3}x_I^3 + \frac{b}{2}x_I^2 + (bc)^{1/2}x_I y_I + \frac{c}{2}y_I^2 + \dots \tag{1.47}$$

with $a > 0$. The image positions are given by Fermat's principle:

$$x_I = \pm\frac{1}{\sqrt{a}}\,[x_S - (\frac{b}{c})^{1/2}y_S]^{1/2}$$

$$y_I = \frac{1}{c}\,y_S - (\frac{b}{c})^{1/2}x_I$$

and each image has magnification:

$$\mathcal{A} = \frac{1}{2acx_I}$$

- if $x_S > (\frac{b}{c})^{1/2}y_S$ there are two images
- if $x_S < (\frac{b}{c})^{1/2}y_S$ there are no images

- if $x_S = (\frac{b}{c})^{1/2} y_S$ the two images merge with infinite amplification at $x_I = 0$, in the direction given by $\frac{dy_I}{dx_I} = -(\frac{b}{c})^{1/2}$. The lines $x_I = 0$ and $x_S = (\frac{b}{c})^{1/2} y_S$ locally represent the critical line and the caustic.

For the *cusp catastrophe* the time surface is locally:

$$\tau(\underline{\theta}_I) = \frac{a}{4} x_I^4 + \frac{b}{2} x_I^2 y_I + \frac{c}{2} y_I^2 + \dots \tag{1.48}$$

The image positions are the solutions of the equations:

$$a x_I^3 + b x_I y_I = x_S$$

$$\frac{b}{2} x_I^2 + c y_I = y_S$$

with magnifications:

$$\mathcal{A} = \frac{1}{(3ac - b^2) x_I^2 + bc y_I}$$

The caustic is given by the condition $\mathcal{A} \to \infty$:

$$y_S^3 = \frac{27c^2}{8b} (1 - 2\frac{ac}{b^2}) x_S^2$$

and the critical line is:

$$y_I = (\frac{b^2 - 3ac}{bc}) x_I^2$$

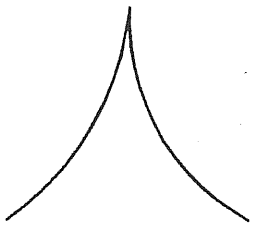

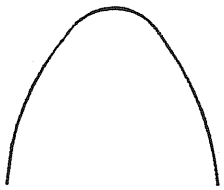

caustic (source plane) critical line (image plane)

Fig. 11

Moving a source with the lens fixed, the images become elongated parallely to the critical line. when $\underline{\theta}_S = \underline{0}$ the three images merge simultaneously at $\underline{\theta}_I = \underline{0}$ in a very bright image ($\mathcal{A} \to \infty$) at the same location (a source in the region "inside" the cusp gives three images, a source "outside" only one image).

- If $b^2 < 2ac$ (*positive cusp*) two positive parity images and a saddle point merge to leave a positive parity image; this cusp is produced by the shrinking of a lemniscate to a point;
- if $b^2 > 2ac$ (*negative cusp*) one positive-parity image and two negative-parity saddle points merge to leave a saddle point.

In general cusp catastrophes consist of only a small fraction of the total length of caustics (however this can not be true when many microlenses are considered all together). *Higher order catastrophes* occur with even smaller frequency; varying the source redshift one has three *control parameters*[2], and three more types of caustic, the *swallow-tail, elliptic umbilic* and *hyperbolic umbilic* catastrophes. Cusp catastrophes form lines in this 3-dimensional space, and fold catastrophes form sheets.

THE PROPAGATION FORMALISM

This term includes several approaches. The propagation of light in an inhomogeneous universe with no well defined lens plane is described by the relativistic optical scalar equations (OSE) by Sachs [1961] and Penrose [1966]. Zel'dovich [1964], Bertotti [1966] and Gunn [1967] tried to solve the OSE in a given cosmological model using a perturbation approach. Dyer and Roeder [1972, 1973] used an exact Robertson-Walker metric, considering the effects of clumpiness in the OSE only. Kantowski [1969] and Dyer and Roeder [1974] used an exact solution of Einstein's equations, the "Swiss-cheese model" with opaque clumps. Nottale [1984] solved to lowest order the redshift and beam diameter equations for a radial light ray in a two step vacuole model. Moreover he generalized the "hybrid method" (perturbing the OSE but not the metric) to any density profile to lowest order in redshift, and solved the hybrid OSE for thin lenses at cosmological redshifts.

Consider a bundle of light rays propagating through an inhomogeneous universe and let λ be the affine parameter along rays, and A the beam cross sectional area. The OSE can be written:

$$\frac{d^2\sqrt{A}}{d\lambda^2} - \mathcal{R}\sqrt{A} + \xi^2 A^{-3/2} = 0 \tag{1.49}$$

where $\mathcal{R}$ is obtained from the Ricci tensor and the wave vector k^a:

$$\mathcal{R} \equiv R_{ab}k^a k^b$$

and ξ/A is the shear amplitude [Kantowski, 1969]. Dyer and Roeder [1973] give the equation for a $\Lambda = 0$ Friedmann universe with null shear ($\xi = 0$):

$$(1+z)(1+2q_0 z)\frac{d^2\sqrt{A}}{dz^2} + (q_0 + 3 + 7q_0 z)\frac{d\sqrt{A}}{dz} + 3q_0\sqrt{A} = 0$$

The solution whose vertex lies at the observer ($z = 0$) is the classical Mattig relation:

$$\sqrt{A} \sim \frac{q_0 z + 1 - q_0 + (q_0 - 1)(1 + 2q_0 z)^{1/2}}{q_0^2(1+z)^2}$$

[2] x_S, y_S, and z_S

This holds for a light beam travelling through a uniform fluid. When clumpiness and shear are taken into account the Mattig formula holds in the average, since their effects balance [Weinberg, 1976]. Many works adopt a vacuole model, i.e. an inhomogeneous model consisting of a high density Friedmann solution (describing the lens) separated from the background universe (a low density Friedmann solution) by an empty Schwarzschild solution.

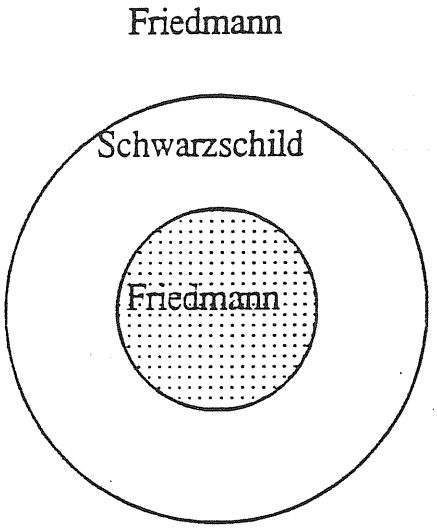

Fig. 12

The density profile must not perturbate the background universe [Eisenstaedt, 1977]. The "diameter" of the beam $\sqrt{A}$ is obtained solving the OSE, and one computes amplification by compairing $\sqrt{A}$ at the lens position and in the external Friedmann solution:

$$Amplification = \frac{\sqrt{A}}{\sqrt{A_F}}$$

This gives an idea of how the propagation formalism works: the thin screen and weak field approximations and the hypotesis of bounded and stationary lens are not needed. The formalism computes the amplification, but it does not reveal itself useful in considering multiple imaging, probability and statistics, and in modelling observed systems.

1.5 MULTIPLE IMAGING

Multiple imaging situations can occur in gravitational lensing. We use the vector formalism with the complex notation and the underlying assumptions; in particular we assume the lens is *smooth, bounded* and *transparent.* The number of images is then constrained by **Burke's theorem** [Burke, 1981] :

> *any smooth,bounded, transparent gravitational lens produces an odd number of images.*

The proof involves parameterization of bent light rays by two direction cosines forming a vector field $\underline{w}$; they reach the observer only for a particular value $\underline{w}^{(0)}$, so the problem is to study the zeroes of the vector field $\underline{w} - \underline{w}^{(0)}$ on the plane; they are constrained by the Poincaré-Hopf index theorem [3]. Burke's theorem can be understood also in the scalar formalism (see before). It also predicts that at least one image with total positive parity ($\mathcal{A} > 0$) is produced, and additional images appear in pairs with $\mathcal{A} > 0$ for one and $\mathcal{A} < 0$ for the other. An equivalent form of Burke's theorem is the following:

> *multiple imaging by a bounded, smooth, transparent lens is possible if and only if there exists a point on the image plane where* $Det(J) < 0$ *(where* J *is the jacobian matrix of the transformation given by the lens equation)*

This formulation is very convenient for obtaining conditions on multiple imaging; the known results can be found in Subramanian and Cowling [1986] and concern mainly symmetric (circular or elliptical) lenses. The results for bounded, smooth, transparent lenses are as follows:

1.5.1 Spherically symmetric lenses

a) The necessary and sufficient condition for a spherically symmetric lens to be capable of multiple imaging is that there exists a point where:

$$2\Sigma - \Sigma_c \overline{\chi} > \Sigma_c$$

Here Σ is the projected surface density of the lens, $\Sigma_c \equiv c^2/4\pi GD$ is the *critical density*, and

$$\overline{\chi} \equiv \frac{\overline{\Sigma}}{\Sigma_c} = \frac{4\pi GD}{c^2} \frac{\int_0^{2\pi} 2\pi b \Sigma(b) db}{r^2}$$

is the mean value of the convergence $\chi \equiv \Sigma/\Sigma_c$.

b) The condition:

$$\exists r_0 : \ \Sigma(r_0) > \frac{\Sigma_c}{2}$$

is *necessary* (but not sufficient) for multiple imaging.

c) For a spherically symmetric lens whose density is maximum at the centre and monotonically decreases outwards, the condition $\Sigma > \Sigma_c$ at the centre is necessary and sufficient for multiple imaging.

[3] All the assumptions are essential in the proof ; it is important to remember this when comparing the result and the observations -see later the "missing image problem"

1.5.2 Elliptical lenses

For an elliptical lens with eccentricity $\sin\beta$ the condition

$$\Sigma(0) > \Sigma_c \frac{1+\cos\beta}{2}$$

is sufficient for multiple imaging.

1.5.3 General lenses

The condition:

$$\exists Q: \ \Sigma(Q) > \Sigma_c$$

is sufficient for multiple imaging.

Decreasing the lens symmetry (from spherical to elliptical), the critical density sufficient for multiple imaging decreases. Examples can be produced showing that there is no lower bound on the surface density Σ necessary for multiple imaging by a general (asymmetric) lens. However these examples are highly unphysical and realistic lenses (galaxies, rich clusters, or stars) probably are not far from being elliptically symmetric in projection, so the comparison of Σ with Σ_c should be indicative of the capability of multiple imaging.

Which objects satisfy $\Sigma > \Sigma_c$? Very roughly, we can consider a lens of mass M and size R as having surface density:

$$\overline{\Sigma} \sim \frac{M}{R^2} \sim 20.8 \left(\frac{M}{10^{11} M_\odot}\right)\left(\frac{R}{1 Kpc}\right)^{-2}$$

Expressing the critical density as:

$$\Sigma_c \equiv \frac{c^2}{4\pi G D} \sim 0.7 \left(\frac{D}{500 Mpc}\right)^{-1} \ g \cdot cm^{-2}$$

we get:

- for a Sun-like star ($M \sim M_\odot$, $R \sim 10^6 Km$):

$$\frac{\overline{\Sigma}}{\Sigma_c} \sim 10^9$$

- for a galaxy ($M \sim 10^{11} M_\odot$, $R \sim 1 Kpc$):

$$\frac{\overline{\Sigma}}{\Sigma_c} \sim 20$$

- for a galaxy cluster ($M \sim 10^{14} M_\odot$, $R \sim 200 Kpc$):

$$\frac{\overline{\Sigma}}{\Sigma_c} \sim 0.6$$

Thus a star or a galaxy at cosmological distance is capable of multiply imaging a distant source, but a cluster would not. However a cluster could influence images created by a single galaxy (e.g. increasing the image separation). It is also possible that two (or more) lenses with subcritical surface densities coming along the line of sight form multiple images of a distant source, even if they are not able to do this singularly. This mechanism has been proposed for lensing by dark galactic haloes [Subramanian *et al.*, 1987]. The probability of lensing should not be negligible and this could account for the observed systems 2345+007 and 1635+267 .

1.6 ARCS FROM GRAVITATIONAL LENSING

Giant, very blue, luminous arcs discovered in rich clusters of galaxies and radio rings are believed to result from gravitational lensing [Paczynski, 1987*a*; Grossman and Narayan, 1988; Narashima and Chitre, 1988]; this can occur when an *extended* source (a galaxy) is lensed, and some of the multiple images merge. If the lens is highly symmetric, the image can be a complete ring, as predicted by Einstein [1936].

1.6.1 Analytical results

We use the vector formalism with polar coordinates (r, ϑ) and (s, ϑ_s) for the image and source positions respectively. Simple lens model are given by Grossman and Narayan [1988]:

a) consider a isothermal sphere with non-singular core, described by the lens potential [Narayan *et al.*, 1984*a*]:

$$\begin{aligned} \Phi_0(r) &= 2\pi\sigma^2 r_c[\tfrac{3}{8}(\tfrac{r}{r_c})^2 - \tfrac{1}{32}(\tfrac{r}{r_c})^4 - \tfrac{21}{32}] \quad if \quad r \leq r_c \\ \Phi_0(r) &= 2\pi\sigma^2 r_c[\tfrac{r}{r_c} - \tfrac{3}{8}\ln(\tfrac{r}{r_c})] \quad if \quad r \geq r_c \end{aligned} \tag{1.50}$$

where σ is the 1-dimensional velocity dispersion and r_c is the core radius of the cluster. The deflection angle is purely radial:

$$\begin{aligned} \alpha_0(r) &= \tfrac{11}{8}\pi\sigma^2\tfrac{r}{r_c} \quad if \quad r \leq r_c \\ \alpha_0(r) &= 2\pi\sigma^2(1 - \tfrac{3r_c}{8r}) \quad if \quad r \geq r_c \end{aligned} \tag{1.51}$$

The caustics in the source plane can be found by imposing $\mathcal{A} = Det(\frac{\partial r}{\partial s}) \to \infty$, and result to be a circle and a central point. The critical lines are circles. When a source is close to a caustic, the images are close to the corresponding critical line and are elongated.

- When an extended source is located on the central caustic point, the images merge forming an *Einstein ring* : this was predicted by Einstein [1936], but he considered point-like sources and lenses, and concluded that the probability of such an event is negligible, since it requires a perfect alignement between source, lens, and observer. The probability becomes higher if one considers extended objects.

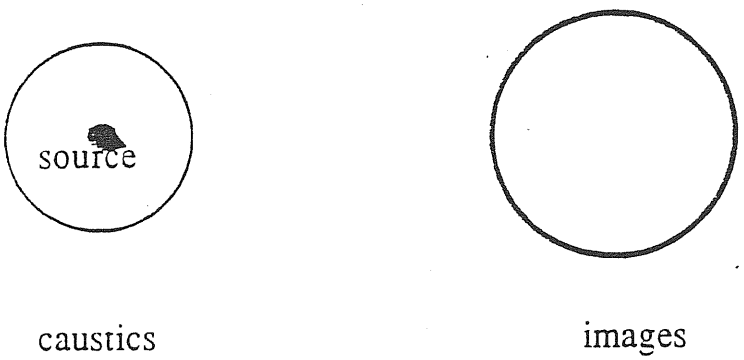

Fig. 13

- When the source is slightly off-center the ring breaks into a *pair* of diametrically opposed arcs:

caustics images

Fig.14

- When the source falls on the outer caustic a radially elongated image appears:

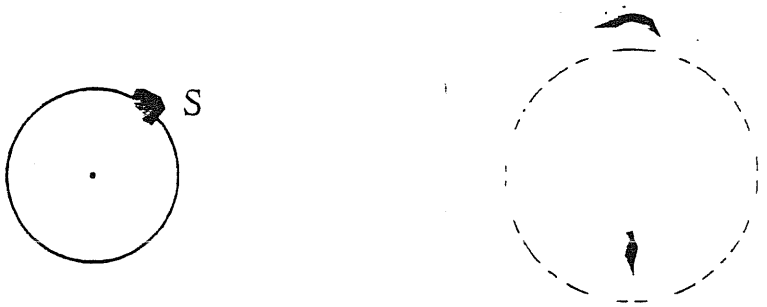

caustics images (solid lines) and critical lines (dotted lines)

Fig. 15

b) A more realistic lens model is described by a monopole plus a quadrupole potential:

$$\Phi = \Phi_0(r) + \varepsilon\Phi_2(r,\vartheta) \equiv \Phi_0(r) + \varepsilon\frac{\pi\sigma^2 r^2\cos(2\vartheta)}{r + r_c} \tag{1.52}$$

where ε is a smallness parameter. The outer caustic (circle) of the spherical case and the associated critical line are deformed into ellipses, while the inner caustic (central point) becomes a diamond-

shaped caustic with four cusps connected by folds. The important feature of this caustic is that it produces single arcs (single giant arcs are observed, with possibly small elongated additional images).

- When an extended source is placed on a cusp of the inner caustic, a single arc (consisting of three merged images) appears, together with two additional very small images:

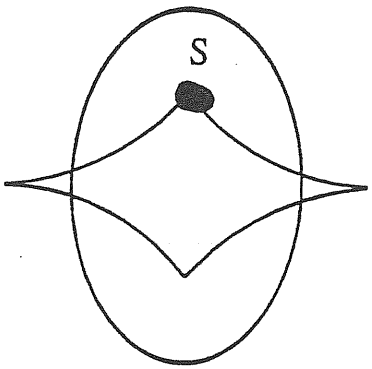

caustics

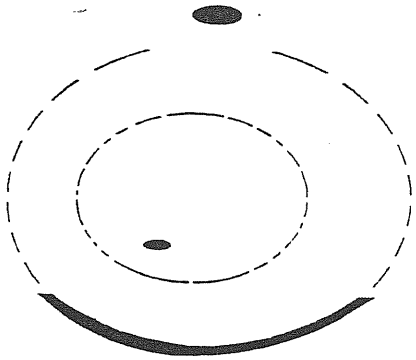

images (solid lines) and critical lines (dotted lines)

Fig. 16

- When the source is on a fold of the inner caustic, substantial arcs are still possible:

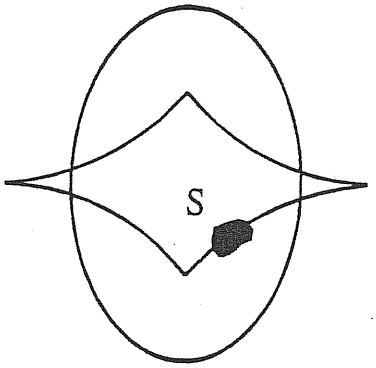

caustics

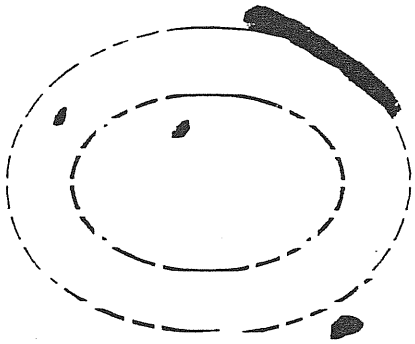

images (solid lines) and critical lines (dotted lines)

Fig. 17

- When the source is on the outer, elliptical caustic, the images are very similar to the corresponding ones for a spherical lens.

Since the caustics separate regions corresponding to different numbers of images, different parts of

an extended source crossing a caustic will give different numbers of images, complicating the resulting figure. The detection of a faint image with the same redshift of the arc would be a good test for the lensing model [Narashima and Chitre, 1988].

1.6.2 Numerical results

Numerical simulations of arcs generation by gravitational lensing have been performed. Grossman and Narayan [1988] generated on a computer a large number of galaxy cluster models, each described by the potential:

$$\Phi(r, \vartheta) = \Phi_0(r) + \varepsilon\Phi_2(r, \vartheta) + \eta\Phi_3(r, \vartheta)$$

where Φ_3 is an octupole term. A probability distribution (believed to be reasonable) for the model parameters is adopted. Each cluster model has large velocity dispersion (since it models a rich galaxy cluster) and a massive galaxy is included at the centre of each cluster. A random configuration of circular background galaxies is created for each cluster model. The results are:

- images as long as the observed arcs occur reasonably often;
- double images are rare in comparison with single ones;
- the arcs are smooth, i.e. the presence of individual galaxies does not cause the arcs to become corrugated.

There are however some problems: the results depend quite sensitively on the choice of the cluster radius r_c; this parameter is poorly determined by the observations. More generous values of r_c than the ones used could be realistic and reduce the frequency of the arcs. Moreover the simulations predict several medium-sized arcs for every long arc discovered; selection effects are clearly operating against the observation of small arcs, but recent results seem to confirm the presence of many elongated small figures together with long arcs [Fort 1988; 1989]. Narashima and Chitre [1988] simulated lensing by a cluster with a massive galaxy at its centre; an extended source is partly single-imaged and partly multiply-imaged. The lens density distribution is smooth and monotonic and one more galaxy is introduced in the cluster to test the effects of graininess by individual galaxies. Long, nearly circular, single arcs occur; the contours in the arcs are distorted only in the neighborhood of the additional galaxy, if it is close enough to the arc.

Apart from the cited problems, these simulations are believed to strongly support the idea that giant blue arcs are generated by gravitational lensing. A test of the lensing model is the measurement of the redshift of the arc, that must be greater than the redshift of the cluster (models alternative to gravitational lensing predict equal redshifts for the arc and the cluster).

Another test has been proposed by Kovner and Paczynski [1988]: since the arcs are very blue, the lensed galaxies should be in a stage of active star formation, with high supernova rates. If any such discrete source varies in intensity, these variations would be reflected in the distant, multiply imaged regions of the arc, with a time delay as short as months or weeks, much shorter than for multiply imaged QSOs.

1.7 MICROLENSING

Lensing by a small mass deflector is called *microlensing* ; realistic microlenses can be stars in galaxies, black holes in halos, etc. Let us consider the order of magnitude of the relevant quantities:

- The **mean deflection angle** by a mass M at distance D for a ray with impact parameter b is roughly:

$$\alpha \sim \frac{M}{b}$$

and

$$\alpha \sim (\frac{M}{D})^{1/2} \sim 10^{-6}(\frac{M}{M_\odot})^{1/2}(\frac{500Mpc}{D})^{1/2} \ arcseconds \tag{1.53}$$

- The **optical depth** for microlensing is $\tau \sim n_* \sigma D$, where n_* is the number of stars per unit angular area, and $\sigma \sim \pi\alpha^2$ is the cross section for the microlensing;

$$\tau \sim n_* \pi \alpha^2 D \sim f_*(\frac{M}{b^2})\frac{1}{\Sigma_c}$$

where f_* is the fraction of local mass in form of microlenses. The local surface density of the galaxy to which microlenses belong is $\Sigma \sim M/b^2$, and roughly:

$$\tau \sim f_* \frac{\Sigma}{\Sigma_c} \tag{1.54}$$

The outer parts of galaxies are optically thin ($\tau << 1$), since $f_* << 1$ and $\Sigma << \Sigma_c$.

The central regions of galaxies are optically thick ($\tau \sim 1$ or $\tau >> 1$), since $f_* \sim 1$ and $\Sigma \sim \Sigma_c$. Therefore in central regions of galaxies one must consider multiple scatterings that make the problem non-linear.

- The microlens is regarded as **point-like** in most works; this is a good approximation since the impact parameter is greater than the radius of a Sun-like star:

$$b \sim (MD)^{1/2} \sim 5 \cdot 10^{15}(\frac{M}{M_\odot})^{1/2}(\frac{D}{500Mpc})^{1/2} \ cm >> r_\odot \sim 10^{11} \ cm$$

- The **timescales** for variations in the images depend on the impact parameter and the source-microlens relative velocity:

$$t \sim \frac{b}{v} \sim \frac{(MD)^{1/2}}{v} \sim 30(\frac{M}{M_\odot})^{1/2}(\frac{D}{500Mpc})^{1/2}(\frac{v}{100Kms^{-1}})^{-1} \ years \tag{1.55}$$

1.7.1 Microlensing at small optical depth

We use the vector formalism and consider a minilens at a time in a general smooth mass distribution (representing a galaxy with possibly a sorrounding cluster). Let I_0 be the scattering function of the smoothed out density distribution and z^i the position of the i-th image prior to microlensing. The lens equation without microlens is:

$$z_S = z^i - \frac{4GD}{c^2} I_0^*(z^i)$$

Introducing a point-like microlens of mass m, the lens equation becomes:

$$z_S = z - \frac{4GD}{c^2} I_0^*(z) - \frac{l_0^2}{(z - z_m)^*}$$

where z_m is the microlens position and

$$l_0 \equiv (\frac{4GDm}{c^2})^{1/2} \sim 3 \cdot 10^{16} (\frac{m}{M_\odot})^{1/2} (\frac{D}{500 Mpc})^{1/2} \ cm \tag{1.56}$$

is the effective radius of influence of the microlens. The function $I_0(z)$ is linearized around the point z^i (since it varies only little on scales $\sim l_0$) and one gets:

$$\frac{l_0^2 \xi}{|\xi|^2} = (1 - \frac{4GD}{c^2} \frac{\partial I_0^*}{\partial z}|_{z^i})(z - z_i) \tag{1.57}$$

where $\xi \equiv \xi_x + i\xi_y \equiv z - z_m$. Eq. (1.57) is the basic equation to be solved for fixed source positions z_m and "old" image positions z^i; its roots ξ give the subimage positions z. Subramanian *et al.* [1985] reduce the problem to solving a quartic equation for the subimage positions. They also find the critical curves in the star plane (x_m, y_m), on which:

$$Det(\frac{\partial z_m}{\partial z}) = 0$$

Crossing the curves, the number of subimages changes from four to two, or possibly from two to zero (or viceversa). Since the scale of angular separation of subimages is $\sim 10^{-6}$ *arcseconds* (far too small to be resolved at present), observations cannot appreciate differences in the number of subimages, except for the vanishing of images and the sudden changes in brightness when two images merge. If a source crosses a fold at t_0, the observed flux decays (or increases) as $|t - t_0|^{-1/2}$ (this is typical in catastrophe theory -see Arnold, 1984). If the source enters a cusp the flux rises again as the source approaches the second fold, giving rise to a typical light curve.

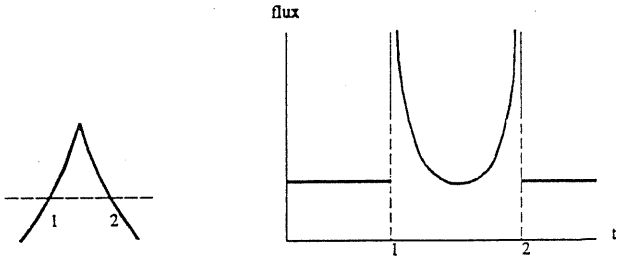

Fig. 18

Amplification on the microcaustic, virtually infinite in the geometric optics approximation, is limited by wave optics and can reach high values that could make microcaustics powerful natural telescopes [Mc Breen and Metcalfe, 1987]. For solar mass stars and a source radius $\sim 10^4$pc (QSO), changes of up to 6 magnitudes may occur [Kayser *et al.*, 1986]. One can, at least in principle, separate intrinsic source fluctuations from microlensing events in multiply imaged systems: the light curve of the microlensed image should differ from the light curves of the other images. Amplification events from microlensing could be an important source of variability in AGNs and BLLac objects [Schneider and Weiss, 1987; Ostriker and Vietri, 1985]. The vanishing of an image is a peculiar feature of microlensing and would be important to detect it [Subramanian *et al.*, 1985; Chang and Refsdal, 1984]. It has been proposed that the missing third image in the double QSO 0957+561 may be due to this effect [Chang and Refsdal,1984]: this has been proposed as a solution of the missing image problem, also for other systems.

Microlensing at small optical depths can be understood also with the scalar formalism [Blandford and Kochanek, 1988]: the character of subimages depends on the form of the time delay surface prior to microlensing.

- If the unperturbed image is at a minimum of the time surface, the isochronal is deformed into a limacon with the maximum located on the microlens, that absorbs the image. Thus there remain *two images*, one at a minimum and one at the saddle point:

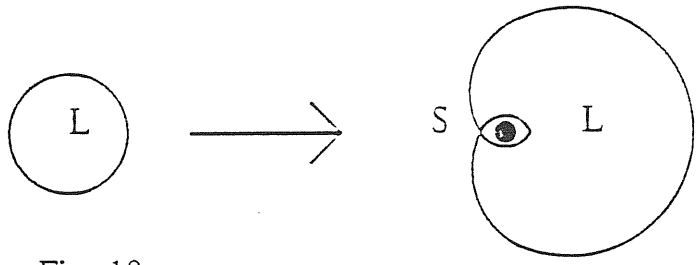

Fig. 19

If the microlens is not point-like but extended, the captured image is so strongly deamplified to be still unobservable [Subramanian *et al.*, 1985].

- If the unperturbed image is at a maximum of the time delay surface, one finds that the unperturbed isochronal is distorted into a lemniscate with two maxima and a saddle point: one of the maxima images is absorbed by the microlens and is unobservable

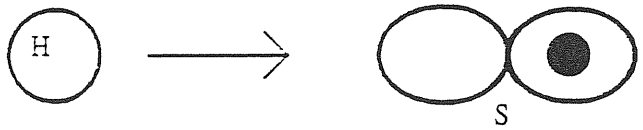

Fig. 20

As a degenerate case, the saddle could merge with the original maximum, annihilating it and leaving only the maximum captured by the microlens.

The second case is the most likely for multiply imaged systems, since maxima are usually associated with dense galactic cores, where the optical depth to microlensing is higher.

1.7.2 Microlensing at large optical depth

At large optical depth a big number of stars is involved and many microlensing events take place. Single microcaustics overlap, forming a caustic network in which the relative occurrence of cusps with respects to folds is higher than for isolated microlenses. There are in principle at least as many subimages as stars in the galaxy, but they have quite different fluxes that decrease with the distance $r_\star$ of a star from the microimage positions as $r_\star^4$ [Schneider and Weiss, 1987; Blandford and Kochanek, 1988]. Because of the many stars involved, numerical simulations are very convenient. Young [1981] applied Monte-Carlo method considering an *extended* source whose light passes through a star field in a galaxy; he investigated the shape of the images, but did not give the amplification factors and the statistics. Paczynski [1986*a*] tried to solve numerically the lens equation for a source behind a random field of stars, in order to find all images. He gave the positions and amplification factors of the subimages, but his method has the following disadvantages (remarked by Schneider and Weiss, 1987):

- it can be applied only to point sources, while the source size is very important in some applications of microlensing theory;
- the method does not guarantee to find all the images (the number of solutions of the lens equation is not known a priori);
- calculations have to be performed for every source position, then the method does not allow statistics (and is very time consuming).

Paczynski's work has been repetead using the ray shooting method [Kayser, 1986]. The features of this work are:

- *extended* sources are considered;
- the error introduced by considering only a limited number of microimages is estimated;
- the total amplification factor is obtained for a whole range of source positions simultaneously;
- the positions of the microimages cannot be obtained; it is claimed that this is not important, since we cannot resolve microimages with the present techniques;
- the work is limited to optical depths $\tau \leq 0.4$

Schneider and Weiss [1987] extended the previous method to large optical depths, determining the amplifications for extended sources with high accuracy, in a scheme useful for statistical considerations (the number of stars considered is up to 10^4). The best accepted results of these simulations are the following:

1. caustics and critical lines strongly tend to cluster in their respective planes; as a consequence, the amplification function is flat on large regions of the source plane;
2. Whereas for moderate optical depths the typical light curve of a source moving relatively to the lens is characterized by rather quiet behaviour most of the time, interrupted by sudden outbursts, sources behind a dense star field show very irregular flickering, without dramatic changes of their apparent luminosities. It can be difficult to separate intrinsic source variations from microlensing effects in observed systems;
3. The effects of the presence of multiple microlenses become sensible even at rather moderate optical depths ($\tau \sim 0.1$).

Kayser *et al.* [1989] explore the effect of considering microlenses *with different masses*: they consider a two-component model composed of massive stars and low mass objects (low mass stars, brown dwarfs, or Jupiters) with mass ratios 1:10 and 1:100. The result is that different masses induce different length scales and the clustering and bridging of caustics and critical lines are enhanced.

1.8 LENSING PROBABILITY AND STATISTICS

The probability of gravitational lensing for distant sources (QSOs) in a realistic universe must be computed theoretically and compared with the observations. In order to do statistical computations we must:

- assume a cosmological model:
- assume a model for statistically relevant lenses, i.e. galaxies, galaxy clusters and microlenses;
- describe the selection procedures by which the source samples are acquired

Press and Gunn [1973] showed that if the universe were composed of point-like masses with density parameter Ω_l, then the probability for a distant point-like source to be significantly amplified is of order Ω_l. This result leads to an overestimate of lensing probability when applied to extended lenses like galaxies or galaxy clusters; these can be characterized by a critical radius r_c such that impact parameters smaller than this will produce multiple images and significant magnifications, but outside r_c the fractional amplification is only $1 + r_c/r$. For typical galaxies r_c is of order a few kiloparsecs, so most of the mass lies outside r_c and is "wasted" with respect to lensing [Vietri and Ostriker, 1983; Ostriker and Vietri, 1986]. Taking this into account, lensing by galaxies should affect about $5 \cdot 10^{-3}$ of all QSOs [Vietri, 1985], an order of magnitude consistent with the observations ($\sim$ 2000 surveyed QSOs and $\sim$ 20 lens candidates). The optical depth to lensing and the expected distributions of image angular separations and lens redshifts (quantities that should be determined by observations) have been computed by Turner, Ostriker and Gott [1984] analytically under the following assumptions:

cosmological model: a standard Friedmann-Robertson-Walker universe with cosmological constant $\Lambda = 0$ and with density fluctuations representing lenses is considered. Three cases are examinated:

- a nearly empty universe with $\Omega << 1$;
- a just closed universe with $\Omega = 1$ and no matter in the optical path aside from the source and the lens (*empty beam case*);
- a just closed universe with $\Omega = 1$ and the beam filled everywhere with matter having the critical density (*filled beam case*)

Redshift z is used as a parameter denoting position along the line of sight. The following quantities are useful:

$$w \equiv 1 + z \; ; \quad x \equiv 1 + z_L \; ; \quad y \equiv 1 + z_S$$

lens model: three cases are considered;

- simple *point masses* describe microlenses;
- *singular isothermal spheres* characterized by a 1-dimensional velocity distribution σ describe galaxies;

– *uniform sheets of matter* describe central regions of galaxy clusters and large scale density inhomogeneities.

source model: only point-like sources (QSOs) are considered.

Each case is treated separately and the results are as follows:

1.8.1 Point masses

The total optical depth to lensing is found to be:

$$\tau = \frac{\Omega_L}{2}\frac{(y-1)^2}{y+1} \quad (\Omega_0 = 0) \tag{1.58}$$

$$\tau = \frac{3}{5}\Omega_L\left[\frac{y^{5/2}+1}{y^{5/2}-1}\ln y - \frac{4}{5}\right] \quad (\Omega_0 = 1) \tag{1.59}$$

According to Press and Gunn [1973], $\tau \propto \Omega_L$. At small redshifts we have:

$$\tau \simeq \frac{\Omega_L}{4} z_S^2 \ (\Omega_0 = 0\,,\ z_S << 1) \tag{1.60}$$

$$\tau \simeq \frac{3}{5}\Omega_L z_S \ (\Omega_0 = 1\,,\ z_S << 1) \tag{1.61}$$

At large redshifts the optical depth saturates, due to the finite distance to the particle horizon:

$$\tau \simeq 0.6\Omega_L(\ln z_S - 0.8) \quad (z_S >> 1) \tag{1.62}$$

The most likely position for a point deflector along the line of sight is given by:

$$(1+z_L)_{max} = (1+z_S)^{1/2} \quad (\Omega_0 = 0) \tag{1.63}$$

$$(1+z_L)_{max} = \{\frac{1}{3}[(1+23y^{5/2}+y^5)^{1/2} - (1+y^{5/2})]\}^{2/5} \quad (\Omega_0 = 1) \tag{1.64}$$

and

$$(z_L)_{max} \simeq \frac{z_S}{2} \quad if \quad z_S << 1 \tag{1.65}$$

in both cases.

The expectation value for image splitting is found to be:

$$\Delta\theta_{rms} = 5.187(\frac{R_L}{R_0})^{1/2}\frac{[y^4(\ln y - 3/4) + y^2 - 1/4]^{1/2}}{(y-1)^2(y+1)^{1/2}} \quad (\Omega_0 = 0) \tag{1.66}$$

$$\Delta\theta_{rms} = 6.703(\frac{R_L}{R_0})^{1/2}\{\frac{y^{7/2}/3(y^{3/2}-1) - y^{5/2}(y-1) + \frac{1}{7}(y^{7/2}-1)}{[\frac{y^{5/2}+1}{y^{5/2}-1}\ln y - \frac{4}{5}](y^{5/2}-1)^2}\}^{1/2} \quad (\Omega_0 = 1) \tag{1.67}$$

where R_L is the Schwarzschild radius of the lens and R_0 is the cosmological scale factor. The expected image separation diverges as $z_L^{-1/2}$ for small z_S and becomes small as $z_S \to \infty$ The optical depth and image separations are shown in figs.21-22

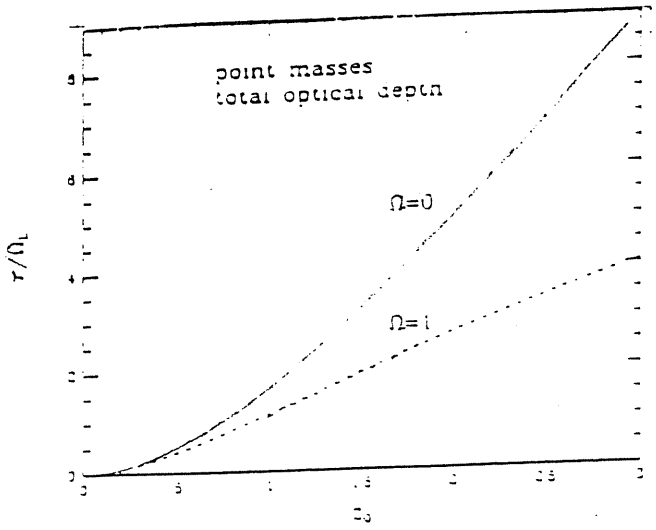

Fig. 21 Optical depth due to lensing by point masses in open and just critical cosmologies, for a point source (from Turner, Ostriker and Gott, 1984)

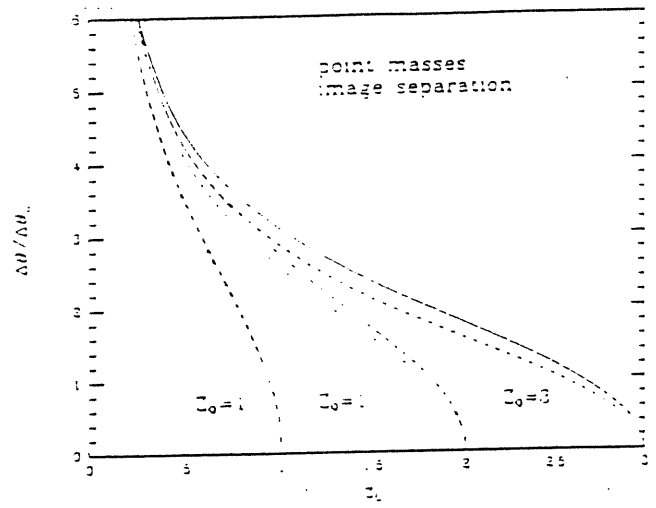

Fig. 22 Root mean square image separation for lensing by point masses (from Turner, Ostriker and Gott, 1984)

1.8.2 Isothermal galaxies

The total optical depth to lensing is found to be:

$$\tau = \frac{F}{4(y^2-1)^2}[(y^4+4y^2+1)\ln y - \frac{3}{2}(y^4-1)] \tag{1.68}$$

$$\tau = \frac{2F}{273}\frac{(y^{1/2}-1)^3}{y^{3/2}}\frac{7y^4+35y^{7/2}+105y^3+193y^{5/2}+230y^2+193y^{3/2}+105y+7}{(y^2+y^{3/2}+y+y^{1/2}+1)^2} \tag{1.69}$$

$$\tau = \frac{4F}{15}\frac{(y^{1/2}-1)^3}{y^{3/2}} \tag{1.70}$$

in the three cases $\Omega_0 = 0$, $\Omega_0 = 1$ empty beam, $\Omega_0 = 1$ filled beam, and where

$$F \equiv 16\pi^3 n_0 R_0^3 (\frac{\sigma}{c})^2$$

where n_0 is the density of lenses and σ the velocity dispersion. We get, for all cases:

$$\tau \simeq \frac{F}{30} z_L^3 \quad if \quad z_L << 1 \tag{1.71}$$

Small redshift QSOs are extremely unlikely to be lensed by an intervening galaxy. The optical depth saturates at $z_L >> 1$:

$$\tau \sim \frac{14}{273}F \quad \Omega_0 = 1 \quad , \; empty \; beam, \quad z_L >> 1 \tag{1.72}$$

$$\tau \sim \frac{4}{15}F \quad \Omega_0 = 1 \quad , \; filled \; beam \; , \quad z_L >> 1 \tag{1.73}$$

Under the most optimistic cosmological assumptions and adopting the value $F = 0.15$ (believed to be physically reasonable), a very large redshift QSO has a 4% chance of being lensed. At realistic redshift $z_S = 2.0$ one gets:

$$\tau = (3.8, 1.6, 2.0) \cdot 10^{-3} (\frac{F}{0.1})$$

in the three cosmological cases. This order of magnitude agrees with the results of Ostriker and Vietri [1986]. The most probable lens position is:

$$(1+z_L)_{max} = [(1+64y^2+y^4)^{1/2} - \frac{1}{6}(1+y^2)^{1/2}]^{1/2} \quad \Omega_0 = 0 \tag{1.74}$$

$$(1+z_L)_{max} = [(1+14y^{5/2}+y^5)^{5/2} - \frac{1}{2}(1+y^{5/2})]^{2/5} \quad \Omega_0 = 1 \quad empty \quad beam \tag{1.75}$$

$$(1+z_L)_{max} = [(5y^{1/2}+1) - \frac{1}{6}(25-34y^{1/2}+25y)^{1/2}]^2 \quad \Omega_0 = 1 \quad filled \quad beam \tag{1.76}$$

One gets:

$$(z_L)_{max} \rightarrow (1.24, 0.55, 0.96) \quad as \quad z_S \rightarrow \infty$$

in the three cases; thus lensing galaxies should have $z_L < 1$. The expected image separation is:

$$< \Delta\theta >= \frac{16}{15}\alpha \frac{(y-1)^5}{(y+1)[(y^4+4y^2+1)\ln y - \frac{3}{2}(y^4-1)]} \qquad (\Omega_0 = 0) \tag{1.77}$$

$$< \Delta\theta >= \alpha \equiv 4\pi(\frac{\sigma}{c})^2 \qquad (\Omega_0 = 1 \ , \ \textit{filled beam}) \tag{1.78}$$

For a given type of lens the expected splitting is nearly independent of the QSO redshift (the y-dependence of $< \Delta\theta >$ in the case $\Omega_0 = 0$ is weak). The typical separation is ~ 2.7 arcseconds, assuming $\sigma \sim 300 Kms^{-1}$.

The optical depth and the image separation for isothermal galaxies are shown in figs. 23-24.

1.8.3 Sheets of matter

In order to produce multiple images, a uniform sheet of matter must have a surface density exceeding the critical value:

$$\Sigma_c = \frac{cH_0}{2\pi G} \frac{x^3(y^2-1)}{(y^2-x^2)(x^2-1)} \qquad (\Omega_0 = 0) \tag{1.79}$$

$$\Sigma c = \frac{5cH_0}{8\pi G} x^4 (y^{5/2}-1)(y^{5/2}-x^{5/2})(x^{5/2}-1) \qquad (\Omega_0 = 1 \ , \ \textit{empty beam}) \tag{1.80}$$

$$\Sigma_c = \frac{cH_0}{8\pi G} \frac{x^2(y^{1/2}-1)}{(y^{1/2}-x^{1/2})(x^{1/2}-1)} \qquad (\Omega_0 = 1 \ , \ \textit{filled beam}) \tag{1.81}$$

An image split by a galaxy (with separation $\Delta\theta_G$) passing through an additional mass sheet with surface density Σ is further separated to angular size $\Delta\theta_{GC}$, where

$$\frac{\Delta\theta_{GC}}{\Delta\theta_G} = \frac{1}{1-\chi} \tag{1.82}$$

The flux amplification is increased to the factor:

$$\frac{\mathcal{A}_{GC}}{\mathcal{A}_G} = \frac{1}{(1-\chi)^2} \tag{1.83}$$

When there are several sheets of matter with density ρ, one has:

$$\chi \equiv \frac{\Sigma}{\Sigma_c} = \int_1^y dw \frac{\rho(w)}{\Sigma_c(w)} \frac{d(ct)}{dw}$$

Usually galaxy clusters have subcritical densities and do not split further the images created by galaxies.

So long as $\tau << 1$ all effects of lensing by different types of objects are linearly superposable. Averages can be performed by weighting different galactic types with coefficients proportional to

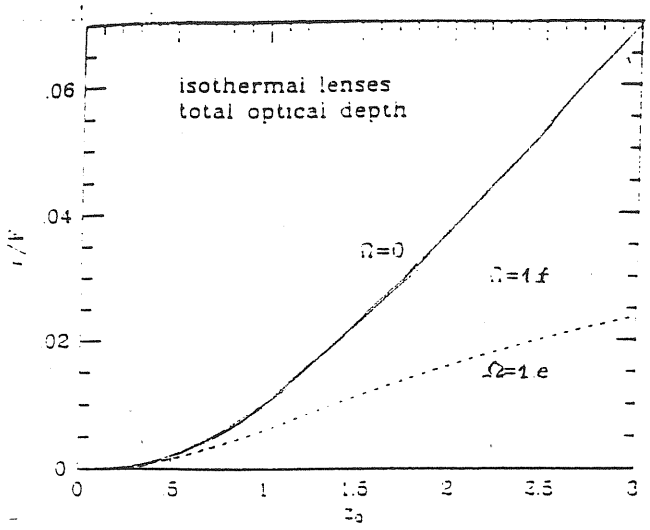

Fig. 23 Optical depth for lensing by singular isothermal spheres (from Turner, Ostriker and Gott. 1984)

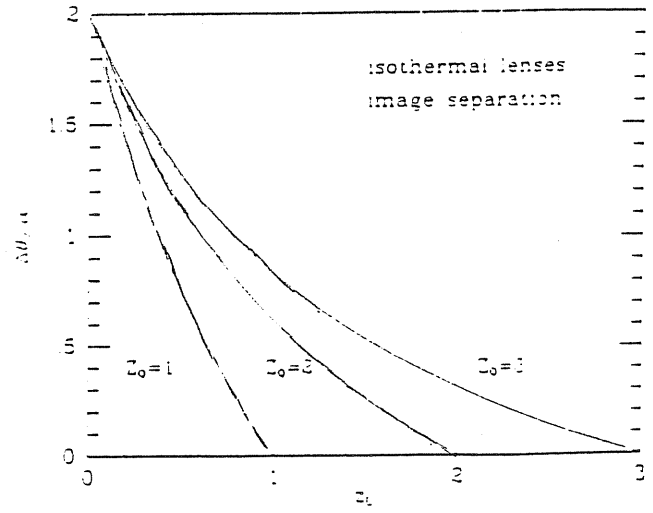

Fig. 24 Image separation for lensing by singular isothermal spheres (from Turner, Ostriker and Gott. 1984).

their luminosities. This is used in a numerical simulation by Turner, Ostriker and Gott [1984]: galaxy clusters and galaxies are considered, with 70%spirals and 30% ellipticals ($\sigma \sim 300 Kms^{-1}$ and $\sigma \sim \frac{300 Kms^{-1}}{\sqrt{2}}$ respectively). The model of the galaxy population is simply a distribution of velocity dispersions and a total overall space density. Multiple imaging by clusters is neglected; 3% of all ellipticals (and no spirals) are assumed to lie in rich cluster cores with $\sigma \sim 1200 Kms^{-1}$ and core radii $r_c \sim 0.2h^{-1}$ Mpc. Sources are point-like QSOs. At least two selection biases affect the observed distributions of $\Delta\theta$ and z_L in observed samples:

- the finite angular resolution of telescopes and detectors biases samples against small $\Delta\theta$ cases;
- the amplification of QSOs flux biases flux-limited samples in favour of the inclusion of lensed QSOs.

The angle selection function (number of QSOs examined for multiple images as function of the limiting angular resolution) is estimated from VLA and optical studies. Rather large amplification biases are taken into account. The expected $\Delta\theta$ and z_L distributions are computed using a sample of 2000 QSOs with redshifts distributed according to the Burbridge-Hewitt catalogue. The results are:

1. the distribution of $\Delta\theta$ in the absence of selection biases is peaked rather sharply at $1''$ and contains very few systems with $\Delta\theta \geq 4''$. Large splittings are rare and due to composite galaxy-plus-cluster lenses;
2. a selection bias resulting from the limiting angular resolution is estimated to give:

$$< \Delta\theta >= 2.53 \ arcseconds \quad if \ \ \Omega_0 = 0$$

$$< \Delta\theta >= 2.32 \ arcseconds \quad if \ \ \Omega_0 = 1 \ , \ filled \ \ beam$$

3. a selection bias favoring highly amplified QSOs in flux-limited samples will cause galaxy-plus-cluster lenses to be overrepresented by a substantial factor. This gives:

$$< \Delta\theta >= 2.32 \ arcseconds \quad (\Omega_0 = 0)$$

$$< \Delta\theta >= 2.50 \ arcseconds \quad (\Omega_0 = 1 \ , \ filled \ beam)$$

4. the combination of the two selection biases is believed to explain the current observations, giving the expectation value:

$$< \Delta\theta >= 3.30 \ arcseconds \quad (\Omega_0 = 0)$$

$$< \Delta\theta >= 3.61 \ arcseconds \quad (\Omega_0 = 1 \ , \ filled \ beam)$$

   The absence of small separation systems in VLA surveys should be regarded as rather surprising;
5. differences in the expected $\Delta\theta$ distributions due to variations in Ω_0 are small and require large, well-understood samples to be detected statistically;

6. the properties of lenses are quite insensitive to even very substantial inhomogeneities in the large scale distribution of matter, unless they approach the critical surface density Σ_c ;
7. the distribution of lens redshifts is peaked near $z_L = 0.5$, with the large majority of cases at $z_L < 1$;
8. the expected number of multiple image systems in the currently observed samples of QSOs is consistent with the observations; large amplifications are to be expected;
9. the results are very sensitive to the adopted central velocity dispersions of galaxies, then to the mass in their cores.

1.8.4 THE PROBABILITY OF ARC LENSING

Extended galaxies can possibly be lensed by rich galaxy clusters, giving images like the giant arcs. Kovner [1987*a*] gives a rough estimate of the probability of arc lensing and the number of expected detectable arcs in the sky. He considers 2000 clusters with redshifts in the range $0.25 \leq z_L \leq 1$ and points out that two conditions must be satisfied in order to obtain arcs such as the observed ones:

- the mass distribution in the lensing cluster must not deviate too much from circularity, a condition probably satisfied by very rich, well-virialized clusters;
- one must consider a cone of astroid cross section (Fig. 25) within which a point source must lie to produce five images. The source galaxy must cover a significant portion of the astroid. Modelling galaxy clusters as isothermal spheres and adopting the available values for their parameters, he finds about 20 arcs similar to the observed ones, a number too large to agree with present observations. More detailed studies by Nemiroff and Dekel [1988] model galaxy clusters as isothermal spheres acting alone and source galaxies as homogeneous circles; their result is that the creation of detectable arcs is of order one over hundreds of nearby rich clusters. Moreover, unusually elongated galaxy images should be much more common than giant arcs. Their existence is predicted also in numerical simulations (see before) and have been observed in A370 [Fort, 1988,1989]. The features of these images are:
  * absence of a dominant central bulge;
  * curved shape along a circle, expecially for images close to the centre of the lensing cluster;
  * major axes perpendicular to the line connecting the image to the cluster centre.

  It should be more likely to finds arcs around distant clusters than around nearby ones. Sources with rather high redshifts are more probable than sources with smaller ones, but the selection effect favoring closer sources with higher surface brightnesses acts against that.

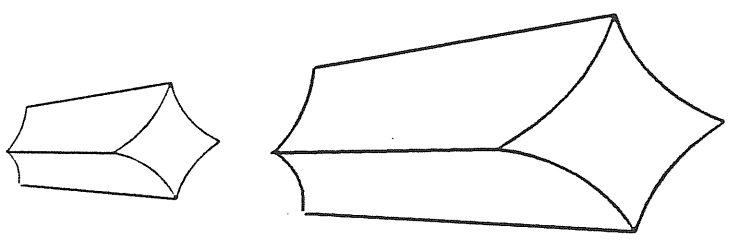

Fig. 25

Chapter 2

OBSERVATIONS

A great deal of observational work followed the discovery of the first gravitational lens candidate in 1979. Today we have three types of observed objects whose existence and structure are explained by gravitational lensing: multiple image systems, giant luminous arcs and radio rings. In addition, gravitational lensing can affect the statistics of QSO surveys, because of the amplification of beams passing near galaxies.

2.1 MULTIPLE IMAGE SYSTEMS

These are the "classical" examples of gravitationally lensed systems. The observational technique to reveal them [Burke, 1986] consists in selecting sources showing multiple, compact structure, and taking optical continuum images with large telescopes; if there is evidence of multiple optical structure, spectra are taken. If the images have identical spectra and redshifts, the system is taken as a strong candidate for lensing. Very good spectra are required to support the lens hypothesis, since QSO spectra are sufficiently similar that, in presence of noise, spectra of different objects show the same features [Shaver and Cristiani. 1987]. If possible, observations are made also in the radio band with VLA and VLBI. Relevant data are the number of images, their relative positions, separations, parities, fluxes, spectra and redshifts, the (eventual) radio structure, the (eventual) observation of the lens, and polarization measurements. Unfortunately, only some systems are radio-loud.

In some cases the lensing object is not observed, leaving place to the possibility of dark matter. An even number of images is most commonly observed, with rather wide splittings ($0.5 - -10$ arcseconds).

Let us consider the various candidates;

2.1.1 0957+561

This is the first discovered [Walsh *et al.*,1979] and best studied lens system. Two images (A and B) of a QSO are observed, with separation $6''$, redshift 1.41 and optical (red) magnitude

$m_A = 17.3$ and $m_B = 17.6$ The lensing galaxy is observed; it is the brightest of a large cluster located near the lens; the cluster centre is not well-determined. The galaxy has redshift 0.36 and magnitude $m = 18.5$ Other galaxies between A and B are ruled out to a limiting r magnitude 25 [Young *et al.*, 1980].

The QSO is radio-loud and has been observed with VLBI and VLA [Booth *et al.*, 1979; Gorenstein *et al.*; Pooley *et al.*,1979; Porcas *et al.*, 1981; Greenfield *et al.*,1985]. VLA observations show a faint radio jet extending from the B image to the core of the lensing galaxy. The extended radio source structure puts some constraints on lens models [Narashima *et al.*, 1984*a*; Greenfield *et al.*, 1985]. VLBI observations show that the two images are possibly similar core-jet sources. The favoured lens model consists of a massive galaxy plus a cluster increasing the image separation ($\sim 2''$ to $6''$). The parities of the two VLBI images agree with this model. The mass of the cluster must include a relevant amount of dark matter that cannot be distributed in the same way as the visible matter [Greenfield *et al.*, 1985]. The expected third image is believed to lie in the galaxy core, where it is deamplified or absorbed [Young *et al.*,1981]. The B image is formed from light passing through the galaxy.

Theoretically predicted time delays are $\sim$ 1 year to 4 years [Dyer and Roeder,1980; Schild, 1986; Gorenstein *et al.*]. A major progress is the measurement of the time delay [Vanderriest *et al.*, 1989], after seven years of photometric monitoring: 415 ± 20 days. Optical light curve data based on a single dip and recovery over hundreds of days give this value. This permits one to obtain a value for the Hubble parameter H_0, that depends on the lens model that one adopts. Unfortunately, the lens cannot be reconstructed uniquely from the image configuration, and this introduce uncertainties in the value of H_0.

2.1.2 PG1115+080

This is the second discovered lens system [Weymann *et al.*, 1980]. We see four images (A, A',B and C) of a QSO at redshift 1.72; A and A' were originally unresolved, their separation being $0.5''$. The fluxes of individual images are not well determined, but approximately $\frac{A}{B} \sim 10$ and $\frac{A}{C} \sim 5$. The whole object has visual magnitude 15.8 and is among the most luminous QSOs in the Schmidt and Green survey [1983]. The separation of the A-A' and B images is $1''.8$, while the A-A' and C separation is $2''.2$. The system is not detectable to the 1.5 mJ flux level with VLA [Weymann *et al.*, 1980].

Early observations could not find the lensing object, however later works report a flux excess (red magnitude 19.8) at the position occupied by the galaxy in lens models [Shaklan and Hege, 1986], and an image that could be a spiral with redshift in the range $0.3 - -0.45$ [Christian *et al.*, 1987].

Lensing models greatly favour lensing by a single galaxy than by a cluster [Narashima *et al.*, 1982]. A five images model with two images nearly coincident at A has been proposed [Young *et al.*, 1981b]. The fifth image is believed to be very faint and to lie in the core of the lensing galaxy [Hege *et al.*,1981].

2.1.3 2016+112

This object consists of three point sources of emission lines, seen also in the radio band [Lawrence *et al.*,1984; Schneider *et al.*, 1985]. Also two galaxies and two extended emission line regions are seen (A, A', B, B', C, C', and D respectively). Their magnitudes are:

$$m_A = 21 \qquad m_B = 21.5$$
$$m_{A'} = m_{B'} = 22.8 \quad m_{C'} = 22.9$$

C is a strong radio source ($m_r \sim 26$); D is probably a giant elliptical galaxy with optical magnitude $m_b = 22.6$ and redshift 1.0 [Schneider *et al.*, 1986]. Spectra of A and B show narrow emission lines at redshift 3.273 . Observations support double lens models, but it is difficult to build simple models giving the three images arrangement (the acute angle ACB is difficult to explain). A five image model has been proposed [Narashima *et al.*, 1984*b*], in which two images merge at C and lensing is due to two galaxies and a cluster at the same redshift 1.01 . In this model the line emission regions A' and B' near the two bright images A and B are distinct sources. VLBI observations should clarify ideas about this model. The expected time delays are in the range $9 - -12$ months.

2.1.4 2237+0305

This system consists of four images of a QSO at redshift 1.69, arranged in a cross-like pattern, separated by less than $1''$ and located in a very large nearby galaxy [Hucra *et al.*, 1985; Tyson, 1986*a*; Yee, 1988]. The lensing galaxy is a luminous Sb barred spiral with redshift 0.0394, velocity dispersion $150 Kms^{-1}$ and magnitude15.7, with a ring and a small bulge [Yee, 1988]. Both the QSO and the galaxy are radio-quiet (up to the limit 0.5 mJ at $\lambda = 6cm$). The fact that the lensing galaxy is so nearby makes 2237+0305 unlike all other known lensed QSOs. The four optical images (originally believed to be a single, strongly amplified QSO) were resolved by Tyson [1986]. Spectra of the four images confirm the QSO spectral nature of at least images A, B, and C [De Robertis and Yee, 1988]. Support to the four images lens model comes from Schneider *et al.* [1988*a*]. Filippenko [1989] reports differences in the M_g II $\lambda 2798$ profile for images A and B; however a possible explanation is that the two images sample slightly different parts of the extended QSO broad line region. A time delay between the images is excluded as an explanation, because it is expected to range from 0.03 days to a few days [Schneider *et al.*, 1988c; Kent and Falco, 1988]. Broad emission line intrinsic variations would require rather long time scales. Very reasonable lens models have been proposed, accounting for most properties of the four images [Schneider *et al.*, 1988*c*; Kent and Falco, 1988] and based on a lensing barred spiral like the one observed. It is not known if these models agree with the possibility of a reported second lensing galaxy at redshift 0.6 [Blandford and Kochanek, 1988]. The fifth image should be absorbed close to the galactic centre. The probability of discovering 2237+0305 by chance is estimated to be $\sim 10^{-2}$ [Kent and Falco, 1988; Blandford and Kochanek, 1988]; such a close alignment between a bright QSO and a nearby galaxy is a rare event, but its probability is raised by the amplification occurring in lensing. The small time delays and the closeness of the

images to the centre of the lensing galaxy make the system the best candidate for monitoring intended to detect microlensing [Kent and Falco,1988; Kayser and Refsdal, 1989]; it should permit obtaining unequivocable results about microlensing.

2.1.5 1146+111

A pair of similar QSOs (B and C) at redshift 1.01 is observed in a region rich of QSOs [Turner *et al.*, 1986] that originally called attention [Hazard *et al.*, 1979]. The separation is 157″. Observations report a possible very distant rich cluster of galaxies between B and C and a number of bright low redshift galaxies in the field between them. The spectra of B and C have been discussed repeatedly; some pairs of spectra show a striking similarity, some other pairs show significant differences. Spectra of B taken at different times by different observers appear to be consistent with the lens hypothesis; this is not the case for the C image [Shaver and Cristiani, 1986; Turner, 1986]. The spectra however are not very relevant, since a time delay of order 10^3 years is expected with any lens model [Blandford and Kochanek 1988]. A mass $\sim 10^{15} M_\odot$ is required by the large B-C separation; it should amplify or multiply image other QSOs in the field, and cause observable dips in the microwave background radiation [Blandford *et al.*, 1987]; however none of these effects has been observed [Blandford *et al.*, 1987; Bahcall *et al.*, 1986]. It is believed that such effects should be observable also if the lens were a supermassive black hole, or a cosmic string, as it has been proposed [Paczynski, 1986*b*; Gott, 1986]. A lensing cosmic string is expected to produce such a large image separation [Vilenkin, 1984]. A less exotic lens could consist in a double galaxy cluster [Crawford *et al.*, 1986; Nemiroff, 1988]. However the evidence for gravitational lensing is poor and the nature of this system is still controversial.

2.1.6 3C324

This is a giant and very luminous radiogalaxy at redshift 1.206; it is one of the most distant objects of this type. The narrow emission line system at $z = 1.206$ seems to consist of two components separated by 1″.1 and possibly two additional faint components. An object at redshift 0.85, possibly a spiral galaxy, is superposed on the other components. Simple gravitational lens models should explain this system [Le Fevre *et al.*, 1987]. The source galaxy probably belongs to a cluster. Large observed overluminosities of very distant radiogalaxies could be due to gravitational amplification [Hammer *et al.*, 1986], and this is probably the case for 3C324 .

2.1.7 2345+007

Two components (A and B) at redshift 2.15 are seen in the optical, with separation 7″.3 [Weedman *et al.*,1982], but there is evidence that B consists of at least two subcomponents [Nieto *et al.*, 1988]. All attempts to observe the lensing object failed. Double lens models have been proposed [Subramanian and Chitre, 1984], but there is no evidence for the cluster or the second nearby galaxy involved; it has therefore been proposed that 2345+007 is the

result of lensing by clumped dark matter with mass $\sim 10^{13} M_{\odot}$ [Tyson *et al.*, 1986]. Other authors believe that this is system is an example of random spatial correlation [Blandford and Kochanek, 1988].

2.1.8 1635+267

This system consists of two QSOs separated by $\sim 4''$. The spectral similarity is not striking: emission line spectra are similar, no velocity difference is measured, and there are clear differences in continuum shape. No lensing object is observed [Djorgowski and Spinrad, 1984]. 1635+267 is a very ambiguous candidate: if it is really lensed, dark matter should be responsible for it. Some authors reject this hypothesis [Blandford and Kochanek, 1988]. Support for the lensing hypothesis comes from spectra obtained with high signal-to-noise ratio [Turner *et al.*, 1988], however further evidences are required.

2.1.9 0023+171

This object was found during a VLA survey searching for new gravitational lenses. Two radio sources (A and B) are seen together with an unresolved source C, with different fluxes. The AB pair and the C image have optical counterparts at redshift 0.94. A very faint extended emission region is seen near the optical C, but there is no evidence for lensing objects. The lens should be visible because it would not be far from us, unless its mass-luminosity ratio is greater than 1000. 0023+171 is then a candidate for lensing by dark matter [Burke, 1986; Blandford and Kochanek, 1988].

2.1.10 PKS1145-071

Two optical images are seen at redshift 1.345, with separation $4''.2$ and similar spectra. The brighter optical image is also a radio source; the other is radio-quiet (the optical/radio luminosities ratio is ≥ 500); no lensing object is observed. The discoverers [Djorgowski *et al.*,1987] and other authors [Blandford and Kochanek, 1988] interpret this object as a physical pair of QSOs; if it is not so, 1145-071 is lensed by dark matter. A double lens model has been proposed [Nemiroff, 1988].

2.1.11 0411+054

This system was discovered in the ongoing gravitational lens survey by Hewitt *et al.* [1986; 1987]. Images are seen in the radio, optical, and near infrared, showing the same structure. The image configuration is a standard one expected for lensing of a point source by an elliptical potential, so very reasonable lens models are possible [Turner,1988]. Good spectra have been obtained, showing an extraordinarily red continuum with no significant emission or absorption features. No extended emission in the red and infrared, as expected from a lensing galaxy at any likely redshift, has been detected. The source point components are

very faint ($m_r \sim 23$); in other words neither the source nor the lens appear to be familiar objects.

2.1.12 1042+178

Radio observations show four images at roughly the vertices of a diamond with length 2″, across the diagonal; one image is sharply brighter than the others. Optical observations cannot resolve the images. Further observations are required.

2.1.13 UM425=1120+019

This system was selected in a optical survey for gravitational lenses, due to its relatively high redshift (1.46) and high apparent luminosity. Optical observations show three close companions (B, C, and D) encircling the bright image A of a QSO. A and B show similar QSO spectra at redshift 1.46. The system has not be seen in VLA observations. Many field galaxies are also observed, suggesting the presence of a rich cluster. Lens models would probably be complicated. Further observations are required [Meylan and Djorgowski, 1989]

2.1.14 3C273

In optical, X, and γ observations this object looks like an abnormally bright QSO. It has a radio core showing superluminal motion at $\sim 10c$. The radio emission occurs in two VLBI components (A and B), the B component coinciding with the optical object. This structure has been explained by lensing with a strong amplification of the QSO core, but weak amplification in the extended radio region [Chitre *et al.*, 1984]. CCD photometry [Tyson *et al.*, 1982] seems to indicate the presence of an elliptical galaxy near the QSO. The lensing model by Chitre *et al.* [1984] is based on the general idea of explaining superluminal sources with gravitational lensing [Chitre and Narlikar, 1979].

2.1.15 H1413+117

Four images of comparable brightness of a broad absorption line QSO are seen in the optical, with separations $\sim 1''$. Two images show identical spectra at redshift 2.55, except for sharp absorption lines present in one component but not in the other. This is explained with gas clouds along the line of sight; other lens systems show this feature. H1413+117 was discovered during a optical search for new gravitational lenses among a sample of bright QSOs [Magain *et al.*, 1988]. Very reasonable lens models seem to describe adequately the image configuration (the so called "cosmic clover leaf"), making 1413+117 a strong candidate for gravitational lensing. Time delays in the range $15 - -350$ days are expected, allowing monitoring this system to detect microlensing effects.

2.1.16 UM673=0142-100=PHL3703

Two images (A and B) of a QSO with R magnitudes $m_A = 16.9$ and $m_B = 19.1$ are observed in the optical at redshift 2.719 and with separation $2''.2$. The spectra are very similar and the lens has probably been observed, looking like a galaxy at redshift 0.49 with magnitude $m_r \sim 19$. Its estimated mass is $\sim 2 \cdot 10^{11} M_\odot$. Time delays of order ~ 7 weeks are expected [Surdej *et al.*, 1987].

2.1.17 0107-025

This system consists of two QSO optical images with separation $77''$, with very similar spectra. No lensing object has been detected. The more recent observations [Surdej *et al.*, 1986] show a redshift difference $\Delta z = 0.004$ between the emission line spectra of A and B; moreover the spectrum of B is steeper in the blue than that of A. These observations, together with the very large A-B separation seem to rule out the gravitational lens hypothesis [Surdej *et al.*, 1986]. However gravitational lens models predict high time delays, so differences in the spectra might not be relevant.

2.2 GIANT ARCS

The discovery of the spectacular giant arcs made a strong impact on the astronomers' community. More than ten such objects are presently known. Their most significant features are:

* location in rich clusters of galaxies;
* narrow arc-like shape and high circularity;
* enormous length ($r \sim 10'' \div 25''$, corresponding to lengths of $\sim 100 Kpc$);
* centre of curvature toward the apparent centre of gravity of the cluster, or a cD galaxy;
* extremely blue color;
* very low surface brightness; the arcs have luminosities comparable with those of E giant galaxies, but are bluer than any cluster member.

The arcs can be satisfactorily explained by gravitational lensing *of an extended galaxy* by *a galaxy cluster* on the line of sight. However alternative models have been proposed [Begelman and Blandford, 1987; Braun and Milgrom, 1989], including tidally stripped galaxies, shock bows, light echo on a thin scattering disk in the cluster core, superconducting cosmic string, etc. As stressed by Paczynski [1987*a*], the essential difference between these models and the gravitational lens is that they predict an arc redshift equal to the redshift of the cluster, while in gravitational lensing the redshift of the arc is greater than the redshift of the cluster. There is spectroscopic evidence supporting the gravitational lensing model for a piece of the arc A370 [Soucail*et al.*, 1988]. Numerical simulations strongly support the lensing model.

With respect to multiple image systems, the giant arcs have some advantages for astronomers and astrophysicists [Turner, 1988]:

* they are relatively easy to find;
* the source is extended and its images can be resolved, so lens models can be constrained;
* typically the lensing cluster can be studied apart from the lensing event, removing some degrees of freedom in the lens models;
* the same cluster may lens more than one background galaxies, providing a test of lensing by varying only the source redshift. However it is very difficult to determine the redshifts of the arcs, due to their low surface brightness.

Let us consider the most spectacular objects:

2.2.1 A370

This object [Soucail *et al.*, 1987; Lynds and Petrosian, 1989] is a long (60^o), narrow arc in the Abell cluster 370 with radius of curvature $15''.1$ and length $21''$, or 143 Kpc at the redshift of the cluster, $z = 0.373$ (assuming $H_0 = 50 Kms^{-1}Mpc^{-1}$, $q_0 = 0.5$ and $\Lambda = 0$). The radial surface brightness distribution is very circular; no evidence for brightness diminution at smaller radii (expected for a shell-like emission) has been found. No systematic narrowing

or dimming of the arc toward its ends is observed; only, the eastern end appears enlarged [Soucail *et al.*, 1987]. The brightness of the arc is $\sim \frac{1}{10}$ of the sky background; the V magnitude is 20.04 and the average surface brightness is 23.2 V mag $arcsec^{-2}$. The intrinsic full width at half maximum varies with color; it is estimated to be 1″.95, 1″.42, 0″.89, 0″.66 and 0″.42 in the U, B, V, R, and I bands respectively. The arc is concave towards both the apparent centre of gravity of the cluster and two cD galaxies with magnitude 19.50. No polarization has been found in the arc. Spectra have been obtained, showing four lines at redshift 0.725 [Lynds and Petrosian, 1989]. Soucail *et al.* [1988] report similar spectra at redshift 0.724; marginal support for these data comes from spectra by Miller and Goodrich [1988]. The arc is not revealed at VLA, but a source is in the vicinity. The variation of the arc width is explained in lensing models assuming that the lensed galaxy is a well-developed Sb spiral with abundance of new star formation in the disk. Fort *et al.* [1988] report several additional structures, faint and elongated objects in the field, bluer than any cluster member; they are believed to be images of galaxies at redshifts ~ 1, the many medium-sized arcs predicted by simulations of lensing by clusters.

2.2.2 Cl2244-02

The arc in this cluster is nearly perfectly circular and is isolated from other normal objects; it appears to be structured, with many prominent knots. The radius of curvature is 10″.6 and the length is 19″, corresponding to 114 Kpc at the cluster redshift 0.328 (assuming $H_0 = 50 Kms^{-1} Mpc^{-1}$, $q_0 = 0.5$ and $\Lambda = 0$). The centre of curvature is towards both the apparent centre of gravity of the cluster and a cD galaxy with V magnitude 19.32; the V magnitude of the arc is 20.09 . There is no significant variation in color along the arc. The average surface brightness is $\sim$ 23.6 V $magnitudes \cdot arcsecond^{-2}$; no polarization has been detected [Lynds and Petrosian, 1989]. Spectral observations are uncertain or report featureless spectra [Lynds and Petrosian, 1989; Miller and Goodrich, 1988]. The object is not observed at VLA, but a double source is in the vicinity. Gravitational lens models predict additional images that possibly have been revealed [Hammer *et al.*, 1988].

2.2.3 A963

Two arcs are observed in this Abell cluster (redshift 0.206), on opposite sides of a cD galaxy, and appear concentric towards its nucleus. The larger arc is to the south of the cD galaxy, 18″.5 from its centre, and subtends an angle of 70° ; the smaller arc is to the north, 12″ from the centre of the cD, and subtends an angle of 30^0. Both arcs are unresolved, and have approximate B magnitudes 22.3 and 23.6 . The arcs are patchy and extremely blue, bluer than any member of the cluster. The cD galaxy is highly elliptical (ellipticity 0.5); one arc (and possibly both) is cut at its middle by the major axis of the cD. Spectra are not available. The image configuration can be obtained with reasonable lensing models [Lavery and Henry, 1988].

2.2.4 Cl0500-24

An elongated structure is seen in this very rich southern cluster at redshift 0.316 . The arc is concave toward a major cluster member, with radius of curvature 26″ and length 14″. The arc is bluer than most galaxies in the cluster. Spectra are not available. The projected structure is located near a close, possibly merging or interacting pair of galaxies at $z = 0.328$ [Giraud, 1988]. At present it seems that a reasonable lens model permits one to obtain the arc [Wambganss *et al.*, 1989]; however further observations are required.

2.2.5 A2218

In this very rich Abell cluster at redshift 0.171 several elongated faint objects are seen; in particular two arcs extend close to both ends of the major axis of a large cD galaxy located at the centre of the cluster, and perpendicular to it. Both arcs are resolved, and are curved with a width of 8 to 10 Kpc (at the cluster redshift). The brightest arc subtends an angle of 30° with centre outside the cD galaxy; the second arc is fragmentary and quite fainter in comparison, consisting of a brighter part A and a faint extension. A is perhaps connected to a second portion A'; the global A-A' system looks like a segment of a roughly circular ring centered outside the cD galaxy, subtending 90°. Another bright galaxy seems to be surrounded by at least two other arcs. The brightest arc is by far bluer than most galaxies, while the second arc is redder (possibly due to contamination from the cD galaxy). Spectra are not available [Pello-Descayre *et al.*, 1989].

2.3 RADIO RINGS

Radio rings constitute the most recently discovered class of lensed systems. *Extended* sources can cross the caustics of a gravitational lens, giving rise to an Einstein ring. Since in galaxies radio emission regions are more extended than optical ones, one expects to see more rings in the radio than in the other bands. Realistic lenses are not circularly symmetric in projection, so the rings will deviate from circularity. The object MG1131+0456 was discovered with VLA [Hewitt *et al.*, 1988]; it is an elliptical ring of emission in radio, accompanied by a pair of more compact, nearly diametrically opposed sources. There is a faint ($m_r = 22$) slightly extended optical counterpart, the spectrum of which shows a continuum, but not emission lines, so its redshift is not available. The ring has clearly defined edges; each of the compact sources (A and B) has substructure: A is double (A_1 and A_2), and B is consistent with being a close double. An additional low surface brightness component C is observed outside the ring . The configuration can be explained assuming that the source is a compact (possibly double) core, accompanied by two radio lobes; one lobe would fall behind the lens and be imaged into the ring; the compact core would fall near enough to the lens to be twice imaged into A_1-A_2 and B. The second lobe would fall far enough from the lens that only one bright image would be visible (C). The lensing potential is clearly non-spherical, since the ring is elliptical. A numerical lens reconstruction technique has been applied to this

system [Kochanek *et al.*,1988]. Another radio ring, MG1654+1346, at redshift 1.7, with a lensing galaxy at $z = 0.25$ is known [Langston *et al.*, 1989]. Radio rings are promising in order to obtain rather well-constrained lens models [Kochanek *et al.*,1988], since they have a brightness distribution, and not only some points. Moreover radio sources frequently have optical counterparts with emission line spectra that make easier to obtain redshift. Thus radio rings can be very useful to determine the lens mass, its detailed distribution, and to test the presence of dark matter.

2.4 PROBLEMS AND FUTURE PROSPECTS

In the class of multiple objects, the systems 0957+561, 1115+112, 2237+0305 , 0142-100 and H1413+117 are believed to be very strong candidates for gravitational lensing. Unfortunately, the image configurations do not allow one to obtain a unique lens model for a given object. Different models (possibly involving double lenses and dark matter) can reproduce an observed image configuration equally well. Only for 2237+0305 the lens model is "reasonably unique", due to the fact that the lensing galaxy is so nearby that it can be studied independently from the lensing event. Moreover our uncertainties about the values of parameters of galaxies and clusters (core radii, velocity dispersions, mass-to-light ratios) do not help in constraining lens models. As a consequence, also the cosmological tests (measure of H_0 and q_0) cannot give precise results, but only rough limits. The situation is different for giant arcs and radio rings, since they could permit to obtain rather detailed lens models, and so a lot of observational work is expected on these systems. We may expect that future observations with the Hubble Space Telescope, Very Large Telescopes, and ISO and XM satellites, with better resolution than the present and limiting magnitudes up to 30 will discover many multiple image systems and medium size arcs, and will help in understanding the already known systems. Efforts with present techniques are also necessary for this purpose and for investigating the statistical galaxy-QSO association. At present a VLA survey is being conducted by Hewitt and collaborators [1986; 1987]. An optical search forms the ESO key programme entitled "Gravitational lensing: quasars and radio-galaxies" [Surdej *et al.*, 1989]. Finally, a good understanding of the statistics of lensing requires a substantial number of confirmed, well understood systems.

Chapter 3

ASTROPHYSICAL APPLICATIONS

Gravitational lensing is very basic for understanding the propagation of electromagnetic waves in our universe, even though the spectacular products like multiple image systems, arcs and rings are rare. Then it is not surprising that lensing theory can be applied to many astrophysical situations. We will give a sketch of the most currently debated topics, together with some problems raised by the observations.

3.1 THE MISSING IMAGE PROBLEM

Burke's theorem predicts an odd number of images from bounded, smooth, transparent gravitational lenses; however in most of the observed multiple systems, an *even* number of images is detected; this constitutes the so-called "missing image problem" [Narashima *et al.*,1986; Narayan *et al.*, 1984*b*; Chang and Refsdal,1984]. One could wonder whether there is really a problem; in fact Burke's theorem is very formal and the assumptions of smoothness and transparency of the lens are essential; they could not be satisfied by realistic lenses. One can dim an image as one wants by introducing in a Burke's lens a compact nucleus that attracts and dims one of the images; in the limit, a singular lens absorbs completely the image (a black hole, or a string, generates *two* images) [Chang and Refsdal, 1984; Blandford and Kochanek, 1988]. Even without appealing to singular lenses, the problem of the missing image could be resolved in some cases by non-transparency due, for example, to dark clouds; this however could not apply in the radio band.Narashima *et al.*[1986] suggest that a compact nucleus (of mass $5 \cdot 10^9 \div 5 \cdot 10^{10} M_\odot$ and size $\leq 50pc$) at the centre of a lens would dim the odd image significantly, without affecting the rest of the image configuration. Consider a spherically symmetric distribution of matter representing the core of the lens galaxy, and add a nucleus of mass M_N and radius R_N, with constant surface density $\Sigma_N = M_N \pi^{-1} R_N^{-2}$. The lens equation (for $|z| < R_N$) turns out to be:

$$z_S = z(1 - \chi_G - \chi_N)$$

where

$$\chi_G \equiv \frac{4\pi G D}{c^2} = \frac{\Sigma_G}{\Sigma_c}$$

$$\chi_N \equiv \frac{4\pi G D M_N}{c^2 R_N^2} = (\frac{R_0}{R_N})^2 = \frac{\Sigma_N}{\Sigma_c}$$

and Σ_G is the central surface density of the galaxy, $R_0 = (4GDc^{-2}M_N)^{1/2}$ is the radius of influence of the nucleus. We denote the position of the source, of the image prior to lensing by the nucleus and of the final images with:

$$z_S = \gamma_S exp(i\theta) \; ; \quad z^I = \gamma^I exp(i\psi) \; ; \quad z = \gamma exp(i\varphi) \tag{3.1}$$

respectively. The locations of the "odd" image without and with the nucleus are respectively:

$$\gamma^I = \frac{\gamma^S}{\chi_G - 1} \quad ; \quad \varphi = \theta + \pi$$
$$\gamma = \frac{\gamma^S}{\chi_G + \chi_N - 1} = \frac{\chi_G - 1}{\chi_G + \chi_N - 1}\gamma^I \quad ; \quad \psi = \theta + \pi$$

(under suitable conditions the nucleus does not create additional subimages [Subramanian *et al.*, 1985]). The amplifications of the odd image without and with the nucleus are:

$$\mathcal{A}^I = \frac{1}{(\chi_G - 1)^2}$$

$$\mathcal{A} = \frac{1}{(\chi_G + \chi_N - 1)^2}$$

Assuming the following parameters:

$$M_G \simeq 5 \cdot 10^{11} M_\odot$$

$$R_{galaxycore} \simeq 3 Kpc$$

$$D \simeq 600 Mpc$$

one gets:

$$\gamma^I \simeq 86\gamma$$

$$\mathcal{A}^I \simeq 3 \cdot 10^{-2}$$

$$\mathcal{A} \simeq 4 \cdot 10^{-6}$$

i.e. introducing the nucleus depresses the "odd" image intensity by a factor of order 10^4 (or ~ 10 magnitudes) and confines the image into the nucleus itself. The properties of the other images are left practically unaltered.

Another possible solution to the missing image problem is that a pair of images are so close together that are seen as a single image. Bray [1984] explores simple models in which the lenses are an E7 and a spiral containing regions corresponding to an even number of images due to the fusion of a pair into one. He finds a closeness of images such that a resolution of 10^{-3} arcseconds is not enough to separate the images.

3.2 THE QSO-GALAXY ASSOCIATION

An excess number of galaxies superimposed on high redshift QSOs is reported. This could hold also for AGNs, X-ray and radio sources. It has been proposed that QSOs lying in directions nearly coincident with some foreground galaxies are magnified by lensing, and hence preferentially included in flux-limited QSOs samples. Schneider [1984] showed that a general mass distribution always enhances the apparent luminosity (of at least one image) of a distant source. Fugmann [1988] presents an automatic galaxy-counting technique claimed to provide non-subjective evidence for QSO-galaxy association. He finds that the number density of relatively bright galaxies increases significantly towards the position of distant ($z_Q > 1$) flat spectrum QSOs. There may also be a less significant excess of galaxies near intermediate redshift QSOs. This result disagrees with the work by Yee and Green [1984], who report no significant QSO-galaxy correlation at $z_Q > 1$; the disagreement may be due to differences in the sample composition [Fugmann, 1988].

Webster *et al.* [1988] consider a completely different QSO sample at $z_Q > 0.5$ and find clear statistical evidence for a greater number of QSO-galaxy juxtapositions than would be expected from random alignments. They also predict that the mass in the foreground lensing galaxies must be substantially greater than is conventionally attributed to a luminous galaxy and its halo. So the phenomenon also supports evidence for the existence of dark matter. It has been noted that the mean density of the universe estimated by Webster *et al.* is too high to be compatible with our knowledge of galaxies [Hogan *et al.*, 1989]. However using the lower bound in their data significantly lowers the mean density of the universe. Increasing the sample size should throw light on the subject [Webster *et al.*, 1989].

Narayan [1989] reexamined the work by Webster and collaborators finding that the reported effect cannot be due to gravitational lensing; however lensing should produce a slightly weaker effect if the limiting magnitude in the survey is corrected.

Kovner [1989] finds a smaller enhancement than Webster and collaborators, but supports the statistical association.

Stocke *et al.* [1987] report the discovery of ten X-ray selected AGNs with relatively high redshifts interpreted as objects significantly brightened by lensing .

Arp [1989] believes that QSO-galaxy association requires a steeper QSO luminosity function than is known, in order to explain the association with microlensing. He and his collaborators argue the physical association of QSOs with low redshift galaxies, and that QSO redshift are not cosmological in origin. However they consider only microlensing, while lensing by galaxies and clusters is surely important for faint magnitude surveys [Narayan, 1989]. This applies also to the work by Linder and Schneider [1988]; they argue that microlensing cannot be held responsible for QSO-galaxy association, due to the fact that the overdensity of QSOs near foreground galaxies depends sensitively on the steepness of the QSO luminosity function, so the known bright QSOs would show a steep luminosity function, but there are only few and the statistics is bad. The amplification of QSO flux should permit to obtain statistical information on the dark halos of galaxies, in particular about their masses [Turner, 1988]; according to Narayan [1989], the effect does not require such

halos to be composed of microlenses (compact objects), but works equally well with smooth density distributions for faint magnitude surveys.

In conclusion, there is not general agreement but it seems that the statistical association between galaxies and high redshift QSOs is real. Analysis of larger QSO samples should confirm it and provide better quantitative results; work is being done in this sense [Webster *et al.*, 1989].

3.3 LENSING AND DARK MATTER

Dark matter affects null geodesics just as luminous matter; we can get information on dark matter in the universe in many ways [Gott, 1987; Turner, 1987]. The multiple systems 2345+007, 1635+267 and 0023+171 , if they are really gravitationally lensed, could provide examples of large amounts of lensing dark matter. Other confirmed systems such as 0957+561 show that a significant amount of non-luminous matter is contained in galactic halos.

3.3.1 Circular velocities in halos

Let us model galaxies as singular isothermal spheres; such a lens gives two bright images [Turner *et al.*, 1984] with separation:

$$\Delta\theta \sim \frac{4GM}{c^2 b} \sim 2\pi(\frac{v_{circ.}}{c})^2 \sim 0''.7(\frac{v_{circ.}}{200 Kms^{-1}})^2$$

where $v_{circ.}$ is the circular velocity in the lensing halo. Since observed multiple systems have image separations in the range $0''.5 - -7''$, we get circular velocities in the range:

$$v_{circ} \sim 170 - -630\, Kms^{-1}$$

Thus observed lensing galaxies have circular velocities larger than the average, or the cluster to which the galaxies belong significantly contribute to the image splitting.

3.3.2 Limits on cosmological density of lenses

The optical depth of the universe to gravitational lensing is roughly:

$$\tau \sim \Omega_{lens}$$

[Press and Gunn, 1973; Turner *et al.*, 1984]. VLBI studies show that most QSOs are not multiply imaged on scales $\sim 10^{-3}$ arcseconds ; image separations are expected to be of order:

$$\Delta\theta \sim 10^{-3}(\frac{M}{10^5 M_\odot})^{1/2}(\frac{D}{1500 Mpc})^{-1/2}\ arcseconds$$

Thus

$$\Omega_{lens} < 1$$

for lenses with masses $M \geq 10^5 M_\odot$. Canizares [1982] examined microlensing of QSO continuum regions: microlensing by objects with masses in the range $0.01 M_\odot - -10^5 M_\odot$ should produce a flux amplification greater for continuum regions than for more extended QSO regions; this is essentially because the amplification decreases with the distance r_* of the light ray from the star as r_*^{-4} [Schneider and Weiss, 1987]. Comparison with the observations permits one to set the limits:

$$\Omega_{lens} < 1$$

for objects with $0.01M_\odot \leq M \leq 10^5 M_\odot$ and

$$\Omega_{lens} < 0.1$$

for objects with $10M_\odot \leq M \leq 10^5 M_\odot$

3.3.3 Constitution of heavy halos

It is believed [Ostriker *et al.*, 1974] that heavy halos surround galaxies, to explain flat rotation curves of galaxies at large radii and the high mass-to-light ratios observed in galaxy clusters. Matter in halos must have a mass-to-light ratio $\frac{M}{L} > 300$ and can be in the form of low mass stars, black holes, nonzero rest mass neutrinos, or other forms of dark matter. If heavy halos composed by low mass stars with $4 \cdot 10^{-4} M_\odot \leq M \leq 0.1 M_\odot$ surround lensing galaxies in the known lens systems, then microlensing should produce fluctuations of order unity in the intensities of QSO images, on time scales $1 - -100$ years [Gott, 1981]. Monitoring the known systems should provide an answer to the question about the constitution of heavy halos. Microlensing by low mass stars should be more easily detectable then microlensing by stellar mass objects, since time delays are shorter.

Rix and Hogan [1988] examine the association between X-ray selected AGNs and foreground galaxies [Stocke *et al.*, 1987] and conclude that it can be understood in terms of dark galaxy halos composed of macroscopic objects with a mean density parameter $\Omega_{lens} > 0.25$.

Evidence against dark matter in form of compact objects with masses $1M_\odot \leq M \leq 3 \cdot 10^4$ is found in 0957+561 and 1115+080 by Subramanian and Chitre [1987]. This comes from studying the intensity ratio of QSO images in different wave bands; microlensing by object in the mass range $10^{-2} M_\odot \leq M \leq 10^4 M_\odot$ amplifies the QSO optical continuum, but not the more extended emission line region. This would result in an increased scatter in the equivalent width of QSO lines and the absence of this effects constraints Ω_{lens}. Comparing the intensity ratio in the optical and the radio puts constraints on the density of dark clusters of stellar mass objects with $M \sim 10^6 M_\odot$. .

If diffuse interstellar or intergalactic matter, or exotic forms of dark matter do not dominate the density of the universe, and objects in galaxies are in the mass range $0.01M_\odot - -10^5 M_\odot$, the limits on the density of lenses can be taken as limits on the mean density of the universe, since gravitational deflection of light is a very basic phenomenon and light rays cannot escape deflection by compact enough aggregates of matter.

3.4 LENSING AND AGNs

BLLac objects are extragalactic, highly variable, polarized sources emitting from the radio to the X band, whose nature is nuclear. They are typically point-like (size less than $2''$), with occasional cases of extended optical or radio emission, have optical continuum spectra steeper than typical QSOs and radio-to-optical ratios higher than typical QSOs. In these features they resemble the optically violently variable QSOs (OVVs), a class of QSOs known for their high polarization and variability. BLLacs are different from OVVs and other QSOs since the normal QSO emission lines are absent or nearly absent. BLLacs are most commonly interpreted as one type of AGNs; however this interpretation suffers problems. Vietri and Ostriker [1985] suggest that a significant part of the BLLac objects are OVVs whose continuum emission has been greatly amplified relative to the line emission by microlenses in intervening galaxies. The estimated percentage of lensed OVVs is about 10%. The process is possible since the size of the extended source is very important in microlensing, and the continuum-emitting region (with size $\sim 10^{15}$ cm) can be lensed with significant amplification , while the larger line emitting region (size $0.1 - -1$ pc) is too large to be strongly influenced by microlenses (stars or black holes in apparently foreground galaxies). The authors believe that normal QSOs are too large, in general, to be affected by microlensing. It is assumed that the stellar spectra seen in either emission or absorption and showing low redshifts (usually attributed to the BLLac object) are due to lensing galaxies. The model contains predictions that, at least in principle, can be tested by the observations. Support for this model comes from numerical studies of microlensing by Schneider and Weiss [1987], who believe that the variability of at least some AGNs can be explained by microlensing events during which amplification varies in time.

3.5 LENSING AND γ-RAY BURSTS

γ-ray bursts appear almost daily in the sky; their origin has been controversial since their discovery [Klebesadel *et al.*,1973]. It seems that the γsources are very close to us (in our Galaxy) or very far from us (at cosmological distances). In the latter case if, for example, they are as far away as QSOs, then they should be gravitationally lensed as frequently as QSOs [Paczynski, 1986*c*]. It seems that one out of 10^3 QSOs is lensed with two or more images separated by $0''.5 - -7''$. From these separations one obtains a light travel time difference between different images ranging from some months to a few years; then it should be possible to see some bursts twice, or a few times. These GRBs should have the same location in the sky, identical spectra and identical γ-ray "light curves", except for different fluxes due to different amplifications. This idea could apply to some observed recurrent GRBs, in particular to the triple repeater B1900+14=GB790324 , obtaining a lens mass of order $10^{10}M_{\odot}$, a reasonable value for an ordinary galaxy. Supermassive black holes ($M \sim 10^6 M_{\odot}$) could cause a double structure in the bursts, due to lensing with a small time delay between different images. It has also been proposed [Paczynski, 1987*b*] that the recurrent soft GRB GB790107 , for which more than 50 bursts were detected, is a single event multiply imaged by a non-random distributions of microlenses. Numerical simulations show that a distribution of bursts clustered in time can be obtained by a spatially clustered distribution of microlenses. All microimages should look similar in the burst duration, time profile and spectrum, although they can differ in intensities and time delays. This is true under the assumption that the sources are point-like and the emission is isotropic.

3.6 MEASURE OF THE HUBBLE PARAMETER

The time delay between two images of a lensed source depends on the mass of the lens and the Hubble parameter. Given the lens model for an observed system, one can in principle measure the time delays between two different images and obtain the Hubble parameter H_0. However, since the choice of the cosmological model affects the theory less than the lens model, and this is not unique for an observed system (see Turner *et al.*,1984; Blandford and Narayan, 1986), the uncertainty on the value of H_0 is big. There is however hope that future observations, expecially of giant arcs and radio rings, will provide really good lens models, permitting a precision in the measure of H_0 better than with the traditional methods.

The time delay between two images of a lensed source is the sum of a geometrical and a gravitational term; in the scalar formalism the time measured by the observer is given by eq. (1.38) :

$$\Delta t(\underline{\theta}_I) = [\frac{D_L D_S}{2D_{LS}}(\underline{\theta}_I - \underline{\theta}_S)^2 - 2\int_S^L \Phi(\underline{\theta}_I)dl](1+z_L)$$

where the angular diameter distances Ds contain the Hubble parameter. Measuring the differences between extremal points of this time surface (corresponding to different images) one gets H_0 [Cooke and Kantowski, 1975; Kayser and Refsdal, 1983; Kayser, 1986; Kovner, 1987*b*]. The best studied gravitational lens candidate to measure time delays is 0957+561; optical light curve data based on a single ~ 0.3 magnitudes dip and recovery over hundreds of days give a delay 415 ± 20 days [Vanderriest *et al.*, 1989]. If this result is correct, and one assumes the lens model by Falco *et al.* [1985], one obtains:

$$H_0 = 86 \;\; Kms^{-1}Mpc^{-1} \;\; \pm 5\%$$

This determination of H_0 is independent of the other known methods. The obtained value is subject to uncertainties coming primarily from the lens model one adopts, and secondarily, it depends on the value of the Ω_0 parameter, and on the presence or absence of mass inhomogeneities in the beam[1] [Kayser, 1986; Blandford and Kochanek, 1988]. However the fact that the value obtained by Vanderriest *et al* lies in the range obtained with the standard methods is very significant.

[1] By emptying or filling the beam one significantly changes the deduced value of H_0

3.7 LENSING BY COSMIC STRINGS

Cosmic strings are topologically stable, one dimensional defects in the vacuum that could form during phase transitions in the early universe. They could possibly be the sources of density fluctuations originating galaxies and galaxy clusters [Zel'dovich, 1980; Vilenkin, 1981]. If they exist at all, cosmic strings could be detected through lensing of extended sources [Vilenkin, 1984; Hogan and Narayan, 1984]. The exterior metric of a cosmic string is described by:

$$ds^2 = -dt^2 + dr^2 + (1 - \frac{4G\mu}{c^2})r^2 d\varphi^2 + dz^2$$

where μ is the linear mass density. Spacetime is locally flat, but has an angle deficit of $4\pi G\mu/c^2$.

Consider a straight string between an observer O and a QSO Q, crossing the line OQ at an angle ϑ; the deflection angle suffered by a light ray is:

$$\delta = \frac{4\pi G\mu}{c^2} \sin\vartheta$$

A straight string produces two images, neither of which is amplified and both with the same parity. This permits one to distinguish between lensing by strings and by conventional gravitational lenses. In a low density universe ($\Omega \sim 0.1$) the image angular separation is expected to be $\delta \sim 100''$, while for a $\Omega \sim 1$ universe $\delta \sim 10''$. Observed angular separations of order $100''$ are hard to explain with conventional objects. Even in a high density universe, one should be able to identify lensing by strings by looking for double galaxies rather than for double QSOs; galaxies are more numerous than QSOs, so one expects to see lines of double galaxies along the strings [Vilenkin, 1984]. Paczynski [1986*d*] argues that if at least one cosmic string exists out to a redshift ~ 1 , it should be discovered during the first year of operation of the Space Telescope, by looking for images *of galaxies*. In fact, if the string passes in front of an extended, resolved, object of angular extent less than $4G\mu/c^2$, it can produce an image with a sharp edge .

Also closed loops have been investigated (but there are indications against the existence of loops on scales significant for lensing [Clarke, Ellis and Vickers, 1988]): if existing, small loops typically produce a pair of magnified merging images.

Since cosmic strings should be irregular and in constant, mildly relativistic, motion or oscillation, and magnified merging images are sensitive to small changes in in the lens, observable variations in the image size, configuration, and total luminosity would occur [Hogan and Narayan, 1984]. A group of four similar twin galaxies has been observed in the optical [Cowie and Hu, 1987], with separations from $2''.0$ to $2''.5$, set in a non-linear arrangement of twins; this group could possibly be attributed to lensing by a cosmic string but much more evidence is required.

3.8 LENSING OF ANISOTROPIES IN THE CMB

Attempts have been made to explain the observed isotropy of the cosmic microwave background (CMB) by gravitational lensing of original inhomogeneities [Kashlinsky, 1988; Linder 1988*a*, 1989]. The problem is important since, in the absence of substantial reheating, CMB permits one to observe the universe as it was at the last scattering epoch ($z_{rec} \sim 1500$). Various cosmological processes that lead to the formation of structures in the universe should have produced fluctuations in the CMB, leaving an imprint by which these processes could be studied [Kayser and Silk, 1986]. Upper limits on the CMB fluctuations can possibly set constraints on the theories of galaxy formation. It is then necessary to know if fluctuations are affected (enhanced or erased) by gravitational lensing due to clumped matter. Since a suitable, realistic, inhomogeneous metric is not known, numerical simulations are performed, or linear perturbations are considered. Kashlinsky [1988] finds that small scale fluctuations of the CMB are significantly attenuated. He estimates that original fluctuations are damped on scales up to several minutes of arc, due to a sort of diffusion process mixing the phases of photons coming from regions at different temperatures. He concludes that theories of galaxy formation are not constrained by observed CMB fluctuations, which are almost erased. This isotropizing effect by gravitational lensing has been found also by Linder [1988*a*], but only at certain scales. On the contrary Sasaki [1988] points out that CMB anisotropies are enhanced on angular scales $\vartheta \leq \vartheta_c$ (where ϑ_c is the correlation angle of the CMB anisotropies), rather than suppressed, if the characteristic deviation angle due to lensing is comparable or greater than ϑ_c; at scales greater than ϑ_c dilution should occur. These results have been successively confirmed by Linder [1988*b*]. The lack of detection of small scale (enhanced) anisotropies in the CMB anisotropies can then constrain the dark matter distribution in the universe.

The impression is however that we still lack a clear vision of the phenomenon on all angular scales.

3.9 LENSING AND SUPERLUMINAL SOURCES

VLBI observations revealed several cases of radio sources with components in their nuclei separating at speeds exceeding the speed of light. These objects can be explained as "illusions", if they are assumed to be at the cosmological distances given by their redshifts. Chitre and Narlikar [1979] proposed an "illusion model" based on gravitational lensing. Consider a radio source consisting of two components A and B, with separation l perpendicular to the line of sight to the observer. Consider also a spherical distribution of matter with mass M and a density profile $\rho(r)$ vanishing for $r > a$. Let light rays pass near this matter distribution with impact parameter r_0 being deflected.

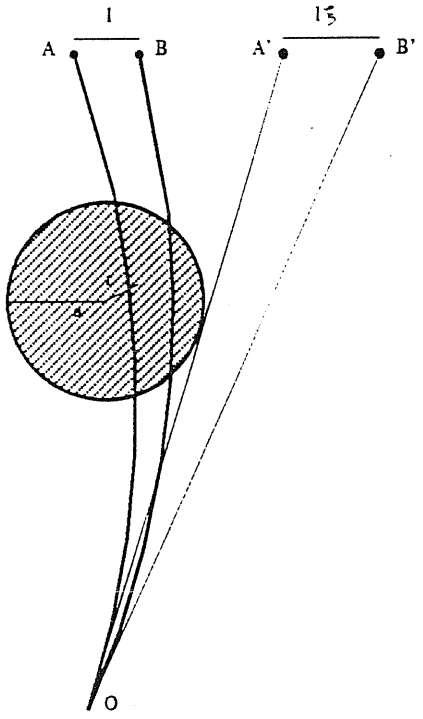

Fig.26

If $r_0 \geq a$ the gravitational bending angle at O is:

$$\alpha(r_0) = \frac{4GM}{c^2 r_0}$$

while if $r_0 < a$ the bending angle is:

$$\alpha(r_0) = \frac{4GM}{c^2 r_0}[1 - \sin\psi + \int_0^{\psi} m(r_0 \sec\varphi)\cos\varphi d\varphi]$$

where $m(r)$ is the fraction of mass contained in the sphere of radius r and

$$\psi \equiv \arccos(\frac{r_0}{a})$$

Since $\alpha(r_0)$ is not constant, the separation of the images A' and B' is different from the separation of the real components A and B, and is given by:

$$l\xi = l[1 - \frac{D_L D_{LS}}{D_S}\alpha(r_0)]^{-1}$$

The factor ξ represents the ratio of the observed separation speed to the real separation speed. For a lensing galaxy it is possible to get $\xi > 1$.

CONCLUSION

Despite its age, gravitational lensing is a developing field of research; it explains the nature, the major features, and in some cases also the details of some astronomical objects by a very basic phenomenon that, no doubt, is very common in a real universe that deviates from a smooth model, even if only the most spectacular events can be appreciated by astronomers. Gravitational lensing theory does not contain exotic aspects, is physically very reasonable and is based on a linear approximation of General Relativity; then its successes are not a test of the full theory. In reality, they are a test of *a class* of theories of gravity: in fact, if we do not take into account cosmology (whose effects on lensed systems are of secondary importance in reproducing image configurations), we can describe gravitational lensing using theories of gravity alternative to General Relativity, and obtaining more or less the same results; one could expect this, since only a weak field approximation is required. More precisely, one can describe gravitation in the post-newtonian limit using the parameterized post newtonian (PPN) formalism, in which ten parameters appear; by suitably assigning their values one specifies the adopted theory of gravity [Will, 1981]. The formulas for the gravitational deflection of light and for time delay contain only one of the ten PPN parameters (γ); its value is 1 in General Relativity as well as in other theories of gravity (Will-Nordtvedt theory, Rosen's bimetric theory, Rastall's theory; other theories are not excluded) [Will, 1981].

There are some theoretical and observational problems: observations of some objects cannot decide if they are really lensed systems or not. For the systems that are most commonly accepted as lensed objects, we cannot provide unique lens models (except for 2237+0305). There is however hope of obtaining well constrained lens models for arcs and rings. The results of lensing theory are only weakly sensitive to cosmology; as a consequence, only rough results can be obtained about this topic from observations. Long monitoring periods are necessary to measure time delays between different images of QSOs (except for H1413+117). Once the time delays are known, the measurement of the Hubble parameter is limited mainly by the non-uniqueness of lens models. However continued monitoring of (possibly several) suitable systems with rather well constrained lens systems can in principle improve the measurement of H_0.

The statistical association between galaxies and QSOs must be examinated with new observations (larger QSO samples). Also the role of lensing in AGNs, BLLac objects, superluminal sources and γ-ray bursts has to be clarified. The theory must also understand the effects of lensing on anisotropies of the CMB, that is now controversial.

Many efforts have been devoted to microlensing; such phenomena can possibly be detected without ambiguities in H1413+117 on reasonable monitoring time scales. Finally, the well-studied system 0957+561 provided evidence of larger velocity dispersions in the centre of galaxies than would be expected, and other evidence for dark matter comes from lensing theory. Some candidates for the role of gravitational lens systems do not show an observable lens; if future observations will confirm them as lens systems, the nature of the lenses will constitute a major puzzle.

It is clear that new instruments such as the Very Large Telescopes and the Hubble Telescope, that will permit one to observe fainter and less separated sources, will be of great help in understanding gravitational lensing. One does not expect new types of objects, but many new multiple image systems (expecially with image separations smaller than those presently known) and small size arcs should be discovered. In fact one expects $\sim 10^6$ QSOs in the sky, and a lensing probability $\sim 10^{-3}$, then $\sim$ 1000 lens systems. These newly discovered systems, though interesting in themselves, will constitute statistically useful samples permitting us to understand, for example, the galaxy-QSO association. Moreover, better observations of the presently known systems should provide many details useful to decide about their nature: if lens systems or not, and for constraining lens models.

One expects to have in rather short times measures of the redshifts of several arcs giving better confirmation of the lens hypothesis. Finally, lensing by cosmic strings should be detected, if they exist at all, during the first years of operation of the Hubble Telescope.

In conclusion, it seems that gravitational lenses will fascinate theoreticians for many years, since they are concrete objects, they link many different fields of astrophysics, and improving the observations promises to solve many problems on non-astronomical timescales.

REFERENCES

Arnold V. I. 1984, *Catastrophe Theory*, Berlin, Springer Verlag

Arp, H. 1989, preprint

Bahcall, J. N. *et al.* 1986, *Nature* **323**, 515

Barnothy, J. M. 1965, *A. J.* **70**, 666

Begelman, M. C. and Blandford, R. D. 1987, *Nature* **330**, 46

Bertotti, B. 1966, *Proc. Roy. Soc. London* **A294**, 195

Berry, M. V. and Upstill, C. 1976, *Progress in Optics XVIII* **2**, 57

Blandford, R. D. and Kochanek, C.S. 1988, in *Proceedings of the 13th Jerusalem Winter School on Dark Matter in the Universe* J. N . Bahcall, T. Piran and S. Weinberg eds., World Scientific, Singapore

Blandford, R. D. and Narayan, R. 1986, *Ap. J.* **310**, 568

Blandford, R. D. *et al.* 1987, *Ap. J.* **318**, 28

Booth, R. S. *et al.* 1979, *Nature* **282**, 385

Bourassa,R. R. and Kantowski, R. 1975, *Ap. J* **195**, 13

Bourassa, R. R. *et al.* 1973, *Ap. J.* **185**, 747

Braun, E. and Milgrom, M. 1989, *Ap. J.* **337**, 644

Bray, I. 1984, *MNRAS* **208**, 511

Burke, W. L. 1981, *Ap. J.* **244**, L1

Burke, B. F. 1986, in *IAU Symp. 119, Quasars*, ed. G. Swarup and V. K. Kapahi, Dordrecht, Reidel

Canizares, C. R. 1982, *Ap. J.* **263**, 508

Carr, B. J. 1980, *A. A.* **89**, 6

Chang, K. and Refsdal, S. 1984, *A. A.* **132**, 168

Chitre, S. M. and Narlikar, J. V. 1979, *MNRAS* **187**, 655

Chitre, S. M. *et al.* 1984, *A. A.* **139**, 289

Christian, C. A. *et al.* 1987, *Ap. J.* **312**, 45

Clarke, C. J. S., Ellis, G. F. R. and Vickers, J. A. 1988, preprint

Cooke, J. H. and Kantowski, R. 1975, *Ap. J.* **195**, L11

Cowie, L. L. and Hu, E. M. 1987, *Ap. J.* **318**, L33

Crawford, C. S. *et al.* 1986, *Nature* **323**, 514

De Robertis, M. M. and Yee, H. K. C. 1988, *Ap. J.* **332**, L49

Djorgowski, S. and Spinrad, H. 1984, *Ap. J.* **282**, L1

Djorgowski, S. *et al.* 1987, *Ap. J.* **321**, L17

Dyer, C. C. and Roeder, R. C. 1972, *Ap. J.* **174**, L115

Dyer, C. C. and Roeder, R. C. 1973, *Ap. J.* **180**, L31

Dyer, C. C. and Roeder, R. C. 1974, *Ap. J.* **189**, 167

Dyer, C. C. and Roeder, R. C. 1980, *Ap. J.* **241**, L33

Einstein, A. 1936, *Science* **84**, 506
Eisenstaedt 1977, *Phys. Rev. D* **16**, 927
Etherington, I. M. H. 1933, *Phil. Mag. Ser 7* **15**, 761
Falco, E. E. *et al.* 1985, *Ap. J.* **289**, L1
Filippenko, A. V. 1989, *Ap. J.* **338**, L49
Fort, B. 1989, in *proceedings of the 12th International Conference on General Relativity and Gravitation*, in press
Fort, B. *et al.* 1988, *A. A.* **200**, L17
Fugmann, W. 1988, *A. A.* **204**, 73
Giraud, E. 1988, *Ap. J.* **334**, L69
Gorenstein, M. V. *et al.* 1988, in *IAU Symp. 129, The Impact of VLBI on Astrophysics and Geophysics*, ed. M. J. Reid and J. M. Moran, Dordrecht, Reidel
Gott, J. R. 1981, *Ap. J.* **243**, 140
Gott, J. R. 1986, *Nature* **321**, 420
Gott, J. R. 1987 in *IAU Symp. 117, Dark Matter in the Universe*, ed. J. Kormendy and G. R. Knapp, Dordrecht, Reidel
Greenfield, P. E. *et al.* 1985, *Ap. J.* **324**, L37
Grossman, S. A. and Narayan, R. 1988, *Ap. J.* **324**, L37
Gunn, J. E. 1967, *Ap. J.* **150**, 737
Hammer, F. *et al.* 1986, *A. A.* **169**, L1
Hammer, F. *et al.* 1988, preprint
Hazard, C. *et al.* 1979, *Nature* **282**, 271
Hege, E. K. *et al.* 1981, *Ap. J.* **248**, L1
Hewitt, J. N. *et al.* 1986*a*, in *Proceedings of the 13th Texas Symp. on Relativistic Astrophysics* ed. M. P. Ulmer, World Scientific, Chicago
Hewitt, J. N. *et al.* 1986*b*, in *IAU Symp. 119, Quasars*, ed. G. Swarup and V. K. Kapahi, Dordrecht, Reidel
Hewitt, J. N. *et al.* 1986*c*, *Nature* **333**, 537
Hogan, C. J. and Narayan, R. 1984, *MNRAS* **211**, 575
Hogan, C. J. *et al.* 1989, *Nature* **339**, 106
Hucra, J. *et al.* 1985, *A. J.* **90**, 691
Kantowski, R. 1969, *Ap. J.* **155**, 89
Kashlinsky, A. 1988, *Ap. J.* **331**, L1
Kayser, R. 1986, *A. A.* **157**, 204
Kayser, R. and Refsdal, S. 1983, *A. A.* **128**, 156
Kayser, R. and Refsdal, S. 1989, *Nature* **338**, 745
Kayser, R. and Silk, J. 1986, *Nature* **324**, 529
Kayser, R. *et al.* 1986, *A. A.* **166**, 36

Kayser, R. *et al.* 1989, *A. A.* **214**, 4
Kent, S. M. and Falco, E. E. 1988, *A. J.* **96**, 1570
Klebesadel, R. W. *et al.* 1973, *Ap. J.* **182**, L85
Kochanek, C. S. *et al.* 1988, preprint
Kovner, I. 1987*a*, *Nature* **321**, 193
Kovner, I. 1987*b*, *Ap. J.* **318**, L1
Kovner, I. 1987*c*, *Ap. J.* **316**, 52
Kovner, I. 1988, preprint
Kovner, I. 1989, *Ap. J.* **341**, L1
Kovner, I. and Paczynski, B. 1988, *Ap. J.* **3 5**, L9
Langston, G. I. *et al.* 1989, preprint
Lavery, R. J. and Henry, J. P. 1988, *Ap. J.* **329**, L21
Lawrence, C.R. *et al.* 1984, *Science* **223**, 46
Le Fevre, O. *et al.* 1987, *Nature* **326**, 268
Linder, E. V. 1988*a*, *A. A.* **206**, 199
Linder, E. V. 1988*b*, preprint
Linder, E. V. 1989, preprint
Linder, E. V. and Schneider, P. 1988, *A. A.* **204**, L8
Lynds, R. and Petrosian, V. 1989, *Ap. J.* **336**, 1
Magain, P. *et al.* 1988, *Nature* **334**, 325
Mc Breen, B. and Metcalfe, L. 1987, *Nature* **330**, 348
Meylan, G. and Djorgowski, S. 1989, *Ap. J.* **338**, L1
Miller, J. S. and Goodrich, R. W. 1988, *Nature* **331**, 685
Narashima, D. and Chitre, S. M. 1988, *Ap. J.* **332**, 75
Narashima, D. *et al* 1982, *MNRAS* **200**, 941
Narashima, D. *et al.* 1984*a*, *MNRAS* **209**, 79
Narashima, D. *et al.* 1984*b*, *Ap. J.* **283**, 512
Narashima, D. *et al.* 1986, *Nature* **321**, 45
Narayan, R. 1986, in *IAU Symp. 119, Quasars*, ed. G. Swarup and V. K. Kapahi, Dordrecht, Reidel
Narayan, R. 1989, *Ap. J.* **339**, L53
Narayan, R. *et al.* 1984*a*, *Nature* **325**, 572
Narayan, R. *et al.* 1984*b*, *Nature* **310**, 112
Nemiroff, R. J. 1988, *Ap. Space Sci.* **145**, 53
Nemiroff, R. J. and Dekel, A. 1988, preprint
Nieto, J. L. *et al.* 1988, *Ap. J.* **325**, 644
Nottale, L. 1984, *MNRAS* **206**, 713
Nottale, L. and Hammer, F. 1984, *A. A.* **141**, 144

Ostriker, J. P. and Vietri, M. 1985, *Nature* **318**, 446
Ostriker, J. P. and Vietri, M. 1986, *Ap. J.* **300**, 68
Ostriker, J. P. *et al.* 1974, *Ap. J.* **199**, L133
Paczynski, B. 1986*a*, *Ap. J.* **301**, 503
Paczynski, B. 1986*b*, *Nature* **321**, 419
Paczynski, B. 1986*c*, *Ap. J.* **308**, L43
Paczynski, B. 1986*d*, *Nature* **319**, 567
Paczynski, B. 1987*a*, *Nature* **325**, 572
Paczynski, B. 1987*b*, *Ap. J.* **317**, L51
Pello-Descayre, R. *et al.* 1989, *A. A.* **190**, L11
Penrose, R. 1966, in *Perspectives in Geometry and Relativity*, ed. B. Hoffman, Bloomington, Indiana University Press
Pooley, G. G. *et al.* 1979, *Nature* **280**, 461
Poston, T. and Stewart, I. N. 1978, *Catastrophe Theory and Its Applications*, London, Pitman
Porcas, R. W. *et al.* 1981, *Nature* **289**, 758
Press, W. H. and Gunn, J. E. 1973, *Ap. J.* **185**, 397
Rix, H. W. and Hogan, C. J. 1988, *Ap. J.* **332**, 108
Rosi, L. A. and Zimmerman, R. L. 1976, *Ap. Space Sci.* **45**, 447
Sachs, R. K. 1961, *Proc. Roy. Soc. London* **264**, 309
Sasaki, M. 1988, preprint
Schild, R. 1986, in *IAU Symp. 119, Quasars*, ed. G. Swarup and V. K. Kapahi, Dordrecht, Reidel
Schmidt, M. and Green, R. F. 1983, *Ap. J.* **269**, 352
Schneider, P. 1984, *A. A.* **140**, 119
Schneider, P. 1985, *A. A.* **143**, 413
Schneider, P. and Weiss, A. 1987, *A. A.* **171**, 49
Schneider, P. *et al.* 1985, *Ap. J.***294**, 66
Schneider, P. *et al.* 1986, *Ap. J.* **91**, 991
Schneider, P. *et al.* 1988*a*, *A. J.* **95**, 1331
Schneider, P. *et al.* 1988*b*, *A. J.* **96**, 1755
Schneider, P. *et al.* 1988*c*, *A. J.* **95**, 1619
Shaklan, S. B. and Hege, E. K. 1986, *Ap. J.* **303**, 605
Shaver, P. A. and Cristiani, S. 1986, *Nature* **321**, 585
Shaver, P. A. and Cristiani, S. 1987, *Nature* **327**, 40
Soucail, G. *et al.* 1987, *A. A.* **184**, L7
Soucail, G. *et al.* 1988, *A. A.* **191**, L19
Stocke, J. T. *et al.* 1987, *Ap. J.* **315**, L11

Subramanian, K. and Chitre, S. M. 1984, *Ap. J.* **276**, 440
Subramanian, K. and Chitre, S. M. 1987, *Ap. J.* **313**, 13
Subramanian, K. and Cowling, S. A. 1986, *MNRAS* **219**, 333
Subramanian, K. *et al.* 1985, *Ap. J.* **289**, 37
Subramanian, K. *et al.* 1987, *MNRAS* **224**, 383
Surdej, J. *et al.* 1986, *A. A.* **161**, 209
Surdej, J. *et al.* 1987, *Nature* **329**, 695
Surdej, J. *et al.* 1989, *The Messenger* No. 55 - March 1989
Turner, E. L. 1986, in *Proceedings of the 13th Texas Symp. on Relativistic Astrophysics*, ed. M. P. Ulmer, World Scientific, Chicago
Turner, E. L. 1987, in *IAU Symp. 117, Dark Matter in the Universe*, ed. J. Kormendy and G. R. Knapp, Dordrecht, Reidel
Turner, E. L. 1988, preprint
Turner, E. L., Ostriker,J. P. and Gott, J. R. 1984, *Ap. J.* **284**, 1
Turner, E. L. *et al.* 1986, *Nature* **321**, 142
Tyson, J. A. 1986, in *IAU Symp. 119, Quasars*, ed. G. Swarup and V. K. Kapahi, Dordrecht, Reidel
Tyson, J. A. *et al.* 1982, *Ap. J.* **257**, L1
Tyson, J. A. *et al.* 1986, *A. J.* **91**, 1274
Vanderriest, C. *et al.* 1989, *A. A.* **215**, 1
Vietri, M. 1985, *Ap. J.* **293**, 343
Vietri, M. and Ostriker, J. P. 1983, *Ap. J.* **267**, 488
Vietri, M. and Ostriker, J. P. 1985, *Nature* **318**, 446
Vilenkin, A. 1981, *Phys. Rev. D* **24**, 2082
Vilenkin, A. 1984, *Ap. J.* **282**, L51
Walsh, D. *et al.* 1979, *Nature* **279**, 381
Wambganss, J. *et al.* 1989, *Ap. J.* **337**, L73
Webster, R. L. *et al.* 1988, *Nature* **336**, 358
Webster, R. L. *et al.* 1989, *Nature* **339**, 106
Weedman, D. W. *et al.* 1982, *Ap. J.* **255**, L5
Weinberg, S. 1972, *Gravitation and Cosmology*, New York, Wiley
Weinberg, S. 1976, *Ap. J.* **208**, L1
Weymann, R. J. *et al.* 1980, *Nature* **285**, 641
Will C. M. 1981, *Theory and Experiment in Gravitational Physics*, Cambridge, Cambridge University Press
Yee, H. K. C. 1988, *A. J.* **95**, 1331
Yee, H. K. C. and Green, R. F. 1984, *Ap. J.* **280**, 79
Young, P. 1981, *Ap. J.* **244**, 736

Young, P. *et al.* 1980, *Ap. J.* **241**, 507
Young, P. *et al.* 1981, *Ap. J.* **244**, 723
Zel'dovich, Ya. B. 1964, *Soviet. Astronomy* **8**, 13
Zel'dovich, Ya. B. 1984, *MNRAS* **192**, 663
Zwicky, F. 1937*a*, *Phys. Rev.* **51**, 290
Zwicky, F. 1937*b*, *Phys. Rev.* **51**, 697